

Spatial Modeling of Savanna Forest Fires

Kimberly Shen

Advised by Professors Simon Levin and Denis Patterson

1 Introduction

Satellite data of tree cover in Sub-Saharan Africa combined with mean annual rainfall (MAR) records have shown that tree cover exhibits a distinctly bimodal distribution in regions with intermediate MAR (1000 to 2000 mm/yr). That is, savannas with low tree cover ($\sim 15\%$) as well as forests with high tree cover ($\sim 80\%$) are frequently observed while intermediate tree cover (50 to 75%) is rarely observed. This bimodal distribution is believed to be a result of the fire interactions with vegetation. For example, incorporation of fire effects into the Staver-Levin model of grass-sapling-forest dynamics allows the model to predict bistability of high and low tree cover states at intermediate MAR in agreement with the data. Thus, it has been suggested that forest and savanna are alternative stable states at intermediate MAR, with savanna stabilized by fire feedback [1, 2].

The bistability of forest and savanna has attracted a significant amount of attention and concern since it suggests that perturbation of forests by climate change, drought, agriculture or other human activity may cause large-scale conversion of forests to savanna which would be difficult to reverse due to hysteresis effects. Forest conservation in turn is crucial contributor to carbon storage and maintenance of forest ecosystem and resources among other things. This motivates a more careful study of the effects of fire on tropical forests. Some shortcomings of previous models of fire in savanna-forest systems are they that have not explicitly modeled fire and/or have not included spatial structure [3–5]. Explicit fire dynamics are also necessary for examining the model on shorter timescales and considering the possible effects of seasonality-dependent flammability on forest dynamics

2 Spatial FGBA Model

Ecologically, the tropical forests that we will be modeling differ markedly from true forests of coniferous trees in several ways. First, savanna trees are not readily killed by fire. Typically, they are only topkilled (i.e. only aerial biomass is burned) and can readily resprout [6–8] or have thickened bark to prevent stem death [9]. Second, fire does not propagate readily through tropical forests [10–12]. Mechanistically, this is due to forest understory shade excluding flammable C4 grasses [9] in addition to reduced wind speeds and increased moisture in the forest microclimate [13, 14]. Lastly, tropical forests have relatively open canopies that do not completely shade out grass [10]. For brevity, we will henceforth refer to tropical forests as “forest” and refer savanna regions with lower tree density as “grassland”.

2.1 Mathematical Description of the Model

We will use a spatially extended Markov jump process to model the dynamics of fires in forest-grass systems. Let $\Omega \subset \mathbb{R}^2$ be the patch of land under study, and let $\{r_i\} \subset \Omega$ be a finite set of N distinct sites contained in the patch of land. The sites can be viewed as locations where a tree or grass patch could potentially grow. Each site r_i undergoes a Markov jump process with states F (forest), G (grass), B (burning), and A (ash) whose transition rates are dependent on the spatial locations and states of all the other sites, $\{r_j \mid j \neq i\} \in \Omega$.

This allows us to model both spatial spreading processes (e.g. forest and fire spreading) as well as non-spatial spontaneous transitions (e.g. fires ignited due to lightning strikes or human activity [15]).

We make the following assumptions in our model: (1) Forests can expand into nearby grass and ash due to local spreading of seeds; (2) Burning areas can expand into nearby forest and grass due to local fire spread; (3) Burning sites are spontaneously quenched into ash at a fixed rate; (4) Grass can regrow spontaneously from ash at a fixed rate due to homogeneous dispersal of grass seeds; (5) Forest can spontaneously transition to grass at a fixed rate due to non-fire related mortality.

Mathematically, we represent these assumptions by allowing each site r_i to transition between the states F, G, B, A at exponentially distributed times with rates given by the sum of spatial spreading (see Table 1) and spontaneous processes (see Table 2). The parameters in the transition rates are defined as follows:

- φ_G, φ_A are constants controlling the rate of forest seeding into grass and into ash, respectively
- β_F, β_G are constants controlling the rate of fire spread within forest and within grass, respectively
- $W_F, W_B : \mathbb{R}^+ \rightarrow \mathbb{R}^+$ are forest spread and burning spread kernels, respectively, which control the extent of spatial spreading as a function of distance between the interacting sites. In general, we assume that the kernels are \mathcal{C}^∞ .

Transition	Rate in discrete system	Ecological process
$G \rightarrow F$	$\frac{\varphi_G}{N} \sum_{j=1}^N W_F(r_i - r_j) \mathbb{1}_{\{X^j(t)=F\}}$	forest spreading into grass
$A \rightarrow F$	$\frac{\varphi_A}{N} \sum_{j=1}^N W_F(r_i - r_j) \mathbb{1}_{\{X^j(t)=F\}}$	forest spreading into ash
$F \rightarrow B$	$\frac{\beta_F}{N} \sum_{j=1}^N W_B(r_i - r_j) \mathbb{1}_{\{X^j(t)=B\}}$	fire spreading into forest
$G \rightarrow B$	$\frac{\beta_G}{N} \sum_{j=1}^N W_B(r_i - r_j) \mathbb{1}_{\{X^j(t)=B\}}$	fire spreading into grass

Table 1: Neighbor spread transition rates

Transition	Rates	Ecological Process
$F \rightarrow G$	μ	non-fire forest mortality
$B \rightarrow A$	q	fire quenching
$A \rightarrow G$	γ	grass regrowth from ash

Table 2: Spontaneous transition rates

A few comments on notational conventions: for the neighbor spread transition rate parameters ($\varphi_G, \varphi_A, \beta_F, \beta_G$) we follow the convention that the subscript is the English letter of the state before the relevant transition while the main letter is the Greek letter of the state after the relevant transition. For the spontaneous transition rates (μ, q, γ) we use greek letters without subscripts. Note that we normalize the neighbor spread rates by $\frac{\text{area}(\Omega)}{N}$ to ensure that the spreading rates remain bounded as $N \rightarrow \infty$.

We will also investigate a different ‘‘cascade’’ mode of vegetation burning in our model based on the burning mechanism proposed by Schertzer et al [4] in addition to the ‘‘diffusion’’ mode of fire spread described by the $W_B(\cdot)$ kernel and β_G, β_F parameters. Assuming that fire spread through a grass-forest land is well-approximated as a percolation process, the flammability of any grass site is expected to increase markedly once the fraction of grass sites in the nearby vicinity of the grass site surpasses the percolation threshold [1, 10, 15], an observation that is also well supported by empirical data [11, 12]. We incorporate this effect by adding the terms

$$\Phi_G\left(\frac{1}{N} \sum_{i=1}^N W_G(r_i - r_j) \mathbb{1}_{\{X^j(t)=G\}}\right) \quad \text{and} \quad \Phi_F\left(\frac{1}{N} \sum_{i=1}^N W_G(r_i - r_j) \mathbb{1}_{\{X^j(t)=F\}}\right) \quad (1)$$

to the $G \rightarrow B$ and $F \rightarrow B$ transition rates of site r_i at time t . Here $W_G : \mathbb{R}^+ \rightarrow \mathbb{R}^+$ is another smooth spreading kernel and $\Phi_G, \Phi_F : \mathbb{R}^+ \rightarrow \mathbb{R}^+$ are smooth sigmoidal functions which output flammability as a function of the local grass cover and the kernel W_G . More explicitly we will assume that $\Phi_G(\cdot)$ and $\Phi_F(\cdot)$ will take the form

$$\Phi_G(x) = g_0 + \frac{g_1 - g_0}{1 + e^{-(x-\theta_G)/s_G}} \quad \text{and} \quad \Phi_F(x) = f_0 + \frac{f_1 - f_0}{1 + e^{-(x-\theta_F)/s_F}}$$

where the parameters are defined as follows:

- f_0, g_0 are the baseline spontaneous flammabilities of forest and grass sites, respectively, when no other grass sites are present due to lightning strikes, human activity, etc. [15]
- f_1, g_1 are the total flammabilities of a grass and forest site, respectively in the limit when the land patch is purely grassland.
- θ_F, θ_G are the percolation thresholds in forest and grass, respectively (we will use $\theta = \theta_F = \theta_G \approx 0.4$ as used for percolation in a square lattice [16]).
- s_F, s_G are non-negative constants controlling the width of forest and grass sigmoids, respectively. The sigmoids are assumed to be nearly step functions so we will set narrow widths of $s_F = s_G = 0.05$

We note that the FGBA model spans multiple distinct timescales. In particular, fire dynamics occur on a time scale of hours, grass regrowth occurs on a time scale of months and forest dynamics occur on a time scale of decades. In particular, we will estimate the parameter values from the expected time between events. Since we assume the transitions occur at an exponential distribution the rates are simply the inverse of the expected time between events. The rate parameters all have the same units of yr^{-1} , and we assume that the vegetation sites are separated by an average distance of 10 m.

The vegetation sites are chosen randomly within a compact square domain $[0, L] \times [0, L] \subset \mathbb{R}^2$ for some fixed $L > 0$. We use periodic boundary conditions to reduce boundary effects and to model an infinite domain. The distance between two points $\vec{r}, \vec{s} \in [0, L] \times [0, L]$ is then computed as

$$|\vec{r} - \vec{s}|^2 = \frac{L}{2\pi} \left(\left[\arg\left(e^{i \frac{2\pi(r_x - s_x)}{L}}\right) \right]^2 + \left[\arg\left(e^{i \frac{2\pi(r_y - s_y)}{L}}\right) \right]^2 \right)$$

where the argument function has range $[0, 2\pi)$.

We will primarily use Gaussian functions for the spreading kernels $W_G(\cdot)$, $W_F(\cdot)$ and $W_B(\cdot)$, although in principle, different functions could be used to model alternative spreading mechanisms if desired. Explicitly, a vegetation site located at \vec{r}_i has spreading kernels

$$W_\square(\vec{r}_j, \vec{r}_i) = \frac{1}{2\pi\sigma_\square^2} \exp\left(-\frac{|\vec{r}_j - \vec{r}_i|^2}{2\sigma_\square^2}\right)$$

where $\square = G, F$, or B . To preserve the physical meaning of the three parameters σ_\square under changes in L and/or N we choose the values of σ_\square to be in units of the average spacing between the vegetation sites in the domain which we define as $\Delta x \equiv \frac{L}{\sqrt{N}}$. The normalization constant of W_\square was chosen that

$$\lim_{N \rightarrow \infty} \frac{1}{N} \sum_{i=1}^N W_\square(\vec{r}_j, \vec{r}_i) = \int_{\Omega} W_\square(\vec{r}_j, \vec{r}_i) d\vec{r}_i \approx \int_{\mathbb{R}^2} W_\square(\vec{r}_j, \vec{r}_i) d\vec{r}_i = 1 \quad (2)$$

where the approximation is valid when $\sigma_\square \ll L$.

The model described in this section is highly similar to the previous models proposed by Hebert-Dufresne et al [17] and Wuyts and Sieber [18] but has several distinctions. First, our model allow the sites the distributed arbitrarily in Ω while [17] and [18] use a square lattice of sites. Our model allows modeling of spatially inhomogeneous vegetation landscapes. Second, [17] and [18] include additional spontaneous transitions $G, A, \rightarrow F$ to model homogeneous long-distance dispersal of forest seeds. Our model incorporates long-distance forest seed dispersal in a more realistic way by allowing the use of an appropriately heavy-tailed kernel for $W_F(\cdot)$. Lastly, [17] and [18] assume that spreading processes occurs strictly via nearest neighbor spreading across adjacent lattice sites while our model allows for more general spreading mechanisms via the spreading kernels.

2.1.1 Parameter estimates

In this section we set reasonable ranges and approximate values for all parameters in the FGBA model. We assume that L represents the physical side length of the area of land under study. Then the average spacing between vegetation sites assuming a uniform probability distribution is $\Delta x \equiv \frac{L}{\sqrt{N}}$. We now estimate the parameter values by considering the case where $\Delta x = 1$ m and $L = 100$ m are fixed, requiring $N = 10^4$.

- A square patch of grassland of side length Δx which is completely surrounded by fire will burn after several minutes. Using Table (1) and Eqn. (2), the burning rate can be approximated as β_G then $\beta_G \approx 10^5$ yr $^{-1}$.
- A square patch of forest of side length Δx which is completely surrounded by fire will burn after about an hour. The burning rate can be approximated as β_F so $\beta_F \approx 10^4$ yr $^{-1}$.
- A burning site is expected to burn for several hours before turning into ash i.e. $q \approx 10^3$ yr $^{-1}$
- An ash site is expected to regrow grass in several months i.e. $\gamma \approx 10^1$ yr $^{-1}$.
- A square patch of grass or ash of side length Δx which is completely surrounded by forest will grow a forest tree after several years to a decade i.e. $\varphi_A \approx \varphi_G \approx 10^0$ to 10^{-1} yr $^{-1}$.
- A tree at a square forest site of side length Δx will spontaneously die from non-fire related causes after about 100 years i.e. $\mu \approx 10^{-2}$ yr $^{-1}$.
- A square grass or forest vegetation site of side length Δx completely surrounded by forest will spontaneously catch fire once every 100 years i.e. $f_0, g_0 \approx 10^{-2}$.
- A grass or forest vegetation site completely will have increased flammability when completed surrounded by grass as compared to forest. We set $f_0 = 10^{-1}$ yr $^{-1}$ and $g_0 = 10^0$ yr $^{-1}$.
- The standard deviation of a fire patch spreading throughout grass or forest vegetation can vary from 1 to 5 m so set $\sigma_B \approx 1$ to 5 m.

- The standard deviation of a forest spreading throughout grass or ash can vary from 1 to 5 m so set $\sigma_B \approx \frac{L}{\sqrt{N}}$ to 1 to 5 m.
- The flammability of a vegetation site is dependent on grass proportions in a 50 m radius up to one standard deviation so $\sigma_G \approx 50$.

We summarize the parameter values and a representative fixed value are given below in Table 3.

Parameter	β_G	β_F	q	γ	φ_A, φ_G	μ	f_0	g_0	f_1	g_1
Estimate	10^4 to 10^6	10^3 to 10^4	10^4	10^1 to 10^2	10^{-1}	10^{-2}	10^{-2}	10^{-2}	10^{-1}	10^0
Value	10^5	10^4	10^4	10^2	10^{-1}	10^{-2}	10^{-2}	10^{-2}	10^{-1}	10^0

Table 3: Estimates and representative values of the parameters for the FGBA model in units of yr^{-1}

In general, we assume that there are three levels of time separation in the rate parameters given by $\beta_G, \beta_F, q > \gamma \gg \varphi_A, \varphi_G, \mu, f_0, g_0$. This concludes our mathematical description of the spatial FGBA model. We summarize the model in the state transition diagram given in Fig. (1) showing the relevant parameters and functions governing transitions between states at each vegetation site.

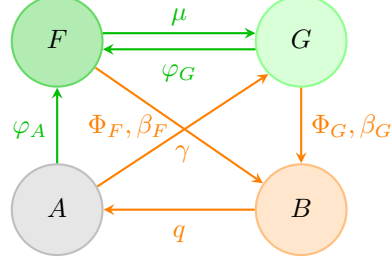


Figure 1: State transition diagram of the spatial FGBA model. Transition arrows are labeled with the relevant parameters and/or flammability functions. Forest and grass/fire timescale transitions are shown in green and orange, respectively.

2.2 Comparison to Mean-Field Approximation

To keep notation as succinct as possible, we will henceforth let $X(r, t)$ indicate the probability that the Markov process at location r and time t is in state X . Note that we will sometimes drop the (r, t) dependence to reduce notational clutter. The full discrete FGBA model including all discussed transition rates in the

previous section result in the following system of equations:

$$\begin{aligned}
\dot{F}(r, t) &= (\varphi_G G + \varphi_A A) \left(\frac{1}{N} \sum_{j=1}^N W_F(r - r_j) \mathbb{1}_{\{X^j(t)=F\}} \right) - \beta_F F \left(\frac{1}{N} \sum_{j=1}^N W_B(r - r_j) \mathbb{1}_{\{X^j(t)=B\}} \right) \\
&\quad - \Phi_F \left(\frac{1}{N} \sum_{j=1}^N W_G(r - r_j) \mathbb{1}_{\{X^j(t)=G\}} \right) F - \mu F \\
\dot{G}(r, t) &= \gamma A - \varphi_G G \left(\frac{1}{N} \sum_{j=1}^N W_F(r - r_j) \mathbb{1}_{\{X^j(t)=F\}} \right) - \Phi_G \left(\frac{1}{N} \sum_{j=1}^N W_G(r - r_j) \mathbb{1}_{\{X^j(t)=G\}} \right) G \\
&\quad - \beta_G G \left(\frac{1}{N} \sum_{j=1}^N W_B(r - r_j) \mathbb{1}_{\{X^j(t)=B\}} \right) + \mu F \\
\dot{B}(r, t) &= (F \Phi_F + G \Phi_G) \left(\frac{1}{N} \sum_{j=1}^N W_G(r - r_j) \mathbb{1}_{\{X^j(t)=G\}} \right) + (\beta_G G + \beta_F F) \left(\frac{1}{N} \sum_{j=1}^N W_B(r - r_j) \mathbb{1}_{\{X^j(t)=B\}} \right) - q B \\
\dot{A}(r, t) &= q B - \gamma A - \varphi_A A \left(\frac{1}{N} \sum_{j=1}^N W_F(r - r_j) \mathbb{1}_{\{X^j(t)=F\}} \right)
\end{aligned}$$

An application of Theorem 2.2.1 in [5] demonstrates that the behavior of the spatial FGBA model in the large land patch limit (i.e. $N \rightarrow \infty$) converges to a solution of the following system of IDEs:

$$\begin{aligned}
\dot{F}(r, t) &= (\varphi_G G + \varphi_A A) \int_{\Omega} W_F(r - r') F(r', t) dr' - \beta_F F \int_{\Omega} W_B(r - r') B(r', t) dr' \\
&\quad - \Phi_F \left(\int_{\Omega} W_G(r - r') G(r', t) dr' \right) F - \mu F \\
\dot{G}(r, t) &= \gamma A - \varphi_G G \int_{\Omega} W_F(r - r') F(r', t) dr' - \Phi_G \left(\int_{\Omega} W_G(r - r') G(r', t) dr' \right) G \\
&\quad - \beta_G G \int_{\Omega} W_B(r - r') B(r', t) dr' + \mu F \\
\dot{B}(r, t) &= (F \Phi_F + G \Phi_G) \left(\int_{\Omega} W_G(r - r') G(r', t) dr' \right) + (\beta_G G + \beta_F F) \int_{\Omega} W_B(r - r') B(r', t) dr' - q B \\
\dot{A}(r, t) &= q B - \gamma A - \varphi_A A \int_{\Omega} W_F(r - r') F(r', t) dr'
\end{aligned}$$

Unfortunately, the spatial model in not analytically tractable. We instead must investigate its behavior using simulations. But first, to gain a rough intuitive understanding of the behavior of the model we will analyze a mean-field approximation of the model which is more analytically tractable. A comparison of the mean-field approximation results to the simulation results will also allow us to examine the impact of spatial structure, which is neglected in the mean-field prediction.

In the mean-field model we assume that the types of states are well-mixed throughout Ω so that interactions depend only on the fractions of land occupied by each state. The system then simplifies to

$$\dot{F}(t) = (\varphi_G G + \varphi_A A) F - \beta_F B F - \Phi_F(G) F - \mu F \tag{3}$$

$$\dot{G}(t) = \gamma A + \mu F - \varphi_G F G - \Phi_G(G) G - \beta_G B G \tag{4}$$

$$\dot{B}(t) = \Phi_G(G) G + \Phi_F(G) F + (\beta_G G + \beta_F F) B - q B \tag{5}$$

$$\dot{A}(t) = q B - \gamma A - \varphi_A F A. \tag{6}$$

The state transition diagram for the spatial FGBA model in the mean field limit is illustrated in Fig. (2). We find the steady states $(\bar{F}, \bar{G}, \bar{B}, \bar{A})$ by setting Equations 3 to 6 all equal to 0 and enforcing the condition that $\bar{F} + \bar{G} + \bar{B} + \bar{A} = 1$. First notice that due to the $G \xrightarrow{\Phi(G)G} B \xrightarrow{qB} A \xrightarrow{\gamma A} G$ cycle then if any one of \bar{G} , \bar{B} , or \bar{A} is nonzero then all three must be nonzero. Next, since there is an $F \xrightarrow{\mu_F} G$ transition then $\bar{F} > 0$ implies $\bar{G} > 0$. Thus, we can classify all steady states as either GBA (where $\bar{F} = 0$ and $\bar{G}, \bar{B}, \bar{A} \neq 0$) or FGBA (where $\bar{F}, \bar{G}, \bar{B}, \bar{A} \neq 0$).

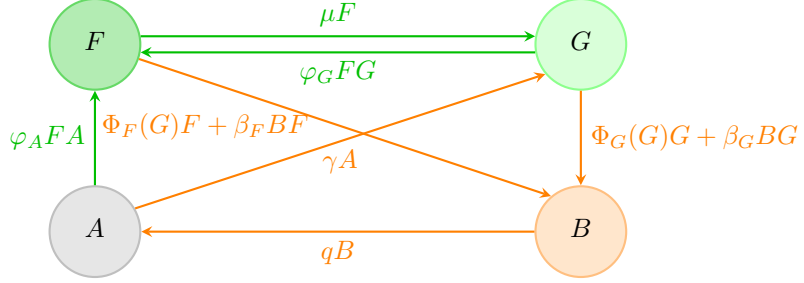


Figure 2: FGBA model state transition diagram in the mean-field limit. Transition arrows are labeled by the transition rates. Forest and fire timescale transitions are shown in green and orange, respectively.

2.3 GBA Steady States

We follow a similar analysis as was performed in [3] and [19]. After setting $F = 0$ and using $A = 1 - G - B$ to eliminate A the system of Equations 3 to 6 can be reduced to

$$\begin{cases} \dot{G}(t) &= \gamma(1 - G - B) - \Phi_G(G)G - \beta_G BG \\ \dot{B}(t) &= \Phi_G(G)G + \beta_G GB - qB. \end{cases} \quad (7)$$

We first claim that for any ecologically relevant initial value (i.e. $G(0) \geq 0, B(0) \geq 0, G(0) + B(0) \leq 1$) that the solution $(G(t), B(t))$ remains ecologically relevant for all times $t \in \mathbb{R}$. Equivalently $(G(t), B(T))$ remains contained in the closed triangle $\mathcal{T}_{GBA} = \{(G, B) \in \mathbb{R}^2 : G \geq 0, B \geq 0, G + B \leq 1\}$ at all times. This is easily shown by observing that the vector field (\dot{G}, \dot{B}) points towards the interior of \mathcal{T}_1 everywhere on $\partial\mathcal{T}_1$:

$$\begin{cases} G = 0 & \Rightarrow \dot{G} = \gamma(1 - B) \geq 0 \\ B = 0 & \Rightarrow \dot{B} = \Phi_G(G)G \geq 0 \\ G + B = 1 & \Rightarrow \dot{G} + \dot{B} = -qB \leq 0. \end{cases}$$

Next we solve for the steady state equilibria of the system by setting both equations in System 7 equal to 0. Solving the system then gives the condition

$$\Phi_G(\bar{G}) = (1 - \bar{G}) \frac{\gamma q}{\gamma + q} \left(\frac{1}{\bar{G}} - \frac{\beta_G}{q} \right) \quad (8)$$

for a steady state (note that division by \bar{G} is a valid operation since $\bar{G} > 0$). Unfortunately, closed form expressions of the equilibria cannot be obtained except in special cases due to the sigmoidal properties of the function Φ_G . However, from this condition it does follow that for any choice of parameter values γ, q , and β_G there is always a unique GBA steady state. To show this we define for convenience

$$\mathcal{F}(G) \equiv (1 - G) \frac{\gamma q}{\gamma + q} \left(\frac{1}{G} - \frac{\beta_G}{q} \right).$$

Then \bar{G} is a steady state if and only if $\mathcal{F}(\bar{G}) = \Phi_G(\bar{G})$. Let us first consider the case where $q < \beta_G$. Then in the interval $[0, 1]$, \mathcal{F} has exactly two roots located at $\frac{q}{\beta_G}$ and 1. Furthermore, $\mathcal{F} > 0$ on $(0, \sqrt{q/\beta_G})$ and $\mathcal{F} < 0$ on $(\sqrt{q/\beta_G}, 1)$. Since $\Phi_G > 0$ on $(0, 1]$ and $0 \leq \Phi_G(0) \leq \infty$ then any roots of $\mathcal{F} - \Phi_G$ in $[0, 1]$ must occur in the interval $(0, q/\beta_G)$. Next note that the derivative of \mathcal{F} is

$$\mathcal{F}'(G) = \frac{\gamma q}{\gamma + q} \left(\frac{\beta_G}{q} - \frac{1}{G^2} \right)$$

and has a single root in $[0, 1]$ located at $\sqrt{q/\beta_G}$. Furthermore, $\mathcal{F}' < 0$ on $(0, \sqrt{q/\beta_G})$. Since $(0, q/\beta_G) \subset (0, \sqrt{q/\beta_G})$ it follows that \mathcal{F} is strictly monotonically decreasing on $(0, q/\beta_G)$. Next since Φ_G is monotonically increasing on $(0, q/\beta_G)$ then $\mathcal{F} - \Phi_G$ is strictly monotonically decreasing on $(0, q/\beta_G)$. Since $\mathcal{F} - \Phi_G$ is continuous on \mathbb{R}^+ and $\lim_{G \rightarrow \infty} (\mathcal{F} - \Phi_G)(G) = +\infty$ while $(\mathcal{F} - \Phi_G)(q/\beta_G) = -\Phi_G(q/\beta_G) < 0$ then $\mathcal{F} - \Phi_G$ must have exactly one root in $(0, q/\beta_G)$. It follows that there is a unique steady state $\bar{G} \in [0, 1]$.

In the case where $q \geq \beta_G$ then \mathcal{F} has exactly one root at 1 in the interval $[0, 1]$ and $\mathcal{F} > 0$ on $(0, 1)$. By the same argument as before $\mathcal{F}' < 0$ on $(0, \sqrt{q/\beta_G})$ so \mathcal{F} is strictly monotonically decreasing on $(0, 1)$. The rest of the argument is the same as the $q < \beta_G$ case with q/β_G replaced by 1. Thus, a unique GBA steady state always exists for any choice of parameters for the system. See Fig. (3) for a graphical illustration.

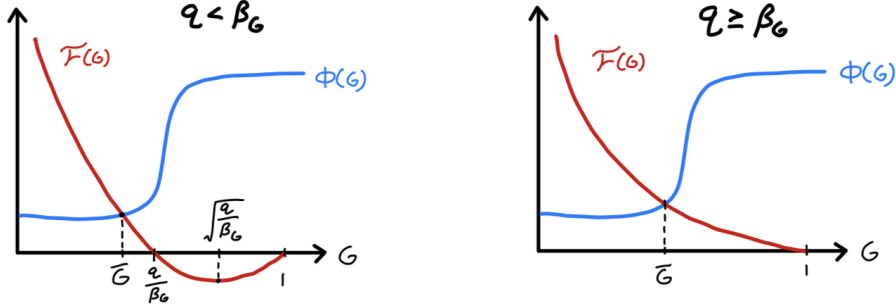


Figure 3: Plots of \mathcal{F} and Φ_G in the $q < \beta_G$ case (left) and the $q \geq \beta_G$ case (right)

Graphically, we note that \bar{G} increases as $\frac{\gamma q}{\gamma + q}$ increases. Noting that $\partial_\gamma(\frac{\gamma q}{\gamma + q}) > 0$ and $\partial_q(\frac{\gamma q}{\gamma + q}) > 0$ when $\gamma, q > 0$ it follows that increasing either γ or q will increase the proportion of grass in the steady state. This is logical since increasing γ allows faster regrowth of grass from ash and increasing q allows faster fire quenching into ash from which grass can regrow. Similarly, increasing $\frac{q}{\beta_G}$ also increases \bar{G} . This also follows intuition: the case of increasing q has already been discussed while decreasing β_G reduces the rate at which grass burns due to fire spread. We also note that increasing g_0 or g_1 reduces \bar{G} as expected since doing so increases the flammability of grass. Lastly, we note that the presence of the GBA steady state depends on the non-decreasing non-tonicity of Φ_G . Thus if Φ_G were constant, the result of the system containing a single unique GBA steady state would still hold.

2.3.1 Stability of the GBA Steady State

In this section we will examine the stability of the unique GBA steady state. We compute the linearization matrix at $F = 0$ of System 7 which gives

$$\mathbf{J}(F = 0, G, B) = \begin{bmatrix} -\gamma - \Phi'_G(G)G - \Phi_G(G) - \beta_G B & -\gamma - \beta_G G \\ \Phi'_G(G)G + \Phi_G(G) + \beta_G B & -q + \beta_G G \end{bmatrix}.$$

The fixed point (\bar{G}, \bar{B}) is stable to perturbations within the $F = 0$ boundary exactly when $J_{F=0}(\bar{G}, \bar{B})$ has eigenvalues with strictly negative real parts. By the Routh-Hurwitz stability criteria this occurs if and only if $\text{Tr}(\mathbf{J}_{F=0}(\bar{G}, \bar{B})) < 0$ and $\det(\mathbf{J}_{F=0}(\bar{G}, \bar{B})) > 0$ [20]. Note that since $\bar{G} < \frac{q}{\beta_G}$ then $-q + \beta_G \bar{G} < 0$ so $\text{Tr}(J_{F=0}(\bar{G}, \bar{B})) < 0$ is clearly satisfied. The condition $\det(\mathbf{J}_{F=0}(\bar{G}, \bar{B})) > 0$ is equivalent to

$$\Phi'(\bar{G}) > \frac{\gamma q}{(\gamma + q)^2} \left(\frac{\beta}{q} - \frac{1}{\bar{G}^2} \right) = \mathcal{F}'(\bar{G})$$

which clearly holds from graphical inspection or more rigorously by recalling from our earlier argument that $\Phi'_G(\bar{G}) \geq 0$ while $\mathcal{F}'(\bar{G}) < 0$. Next to determine whether the GBA fixed point is stable to invasions by F we compute the linearization matrix for the full FGBA system and evaluate it at $F = 0$. We use $A = 1 - F - G - B$ to obtain a dynamical system in the three variables F , G , and B which gives the matrix

$$\mathbf{J}(F=0, G, B) = \begin{bmatrix} \varphi_G G + \varphi_A A - \beta_F B - \Phi_F(G) - \mu & 0 & 0 \\ -\gamma - \varphi_G G + \mu & -\gamma - \Phi'_G(G)G - \Phi_G(G) - \beta_G B & -\gamma - \beta_G G \\ \Phi_F(G) + \beta_F B & \Phi'_G(G)G + \Phi_G(G) + \beta_G B & -q + \beta_G G \end{bmatrix}.$$

The GBA steady state is stable to invasion by F if all the eigenvalues of $\mathbf{J}(\bar{F}=0, \bar{G}, \bar{B})$ have negative real parts. We have already shown that the eigenvalues of the 2×2 submatrix in the lower right have strictly negative real parts so the GBA steady state is stable if and only if the entry in the upper left is negative i.e.

$$\beta_F \bar{B} + \Phi_F(\bar{G}) + \mu > \varphi_G \bar{G} + \varphi_A \bar{A}. \quad (9)$$

An intuitive interpretation of Condition 9 is that the GBA equilibria is resistant to invasion by forest when the rate of tree mortality by fire spread through forest, spontaneous forest fires, and natural mortality exceeds the rate of forest seeding into the steady state grass and ash land. Since a unique GBA steady state exists for any value of the system parameters but its stability can vary based on the parameter values we expect to find transcritical bifurcations within the parameter spaces. In other words, a stable GBA steady state bifurcates into an unstable no-forest state and a stable forest state.

An example bifurcation diagram in $\varphi = \varphi_G = \varphi_A$ using timescale-separated parameter values is given in Fig. (6). As expected, when φ is increased past a critical value, the proportion of forest sites within Ω becomes non-zero. However, the timescale-separated parameter values do produce a mostly ash grassland steady state which is not very ecologically realistic. Nonetheless, it will later be shown that the spatial FGBA model has grassy steady states distinct from the ashy, spatially-homogeneous GBA steady state.

We can slightly generalize the result above to deduce the stability of any GBA state to invasion by forest. In particular, suppose forest invades a trajectory $(0, G(t), B(t), A(t))$ in the $F = 0$ subspace, resulting in the perturbation $(\varepsilon f(t), G(t) + \varepsilon g(t), B(t) + \varepsilon b(t), A(t) + \varepsilon a(t))$. Then to first order in ε :

$$\dot{f}(t) = (\varphi_G G(t) + \varphi_A A(t) - \beta_F B(t) - \Phi_F(G(t)) - \mu)f(t).$$

Separating variables and enforcing initial condition $f(0) = f_0$ then gives

$$f(t) = f_0 \exp \left(\int_0^t ((\varphi_G G(s) + \varphi_A A(s) - \beta_F B(s) - \Phi_F(G(s)) - \mu) ds) \right).$$

Thus, a sufficient condition for the GBA trajectory to be asymptotically stable to invasion by forest is

$$\begin{aligned} \mu &> \sup_{t \in [0, \infty)} \left(\frac{1}{t} \int_0^t ((\varphi_G G(s) + \varphi_A A(s) - \beta_F B(s) - \Phi_F(G(s)))) ds \right) \\ &= \sup_{t \in [0, \infty)} \left(\varphi_G \langle G(t) \rangle_t + \varphi_A \langle A(t) \rangle_t - \beta_F \langle B(t) \rangle_t - \langle \Phi_F(G(t)) \rangle_t \right) \end{aligned}$$

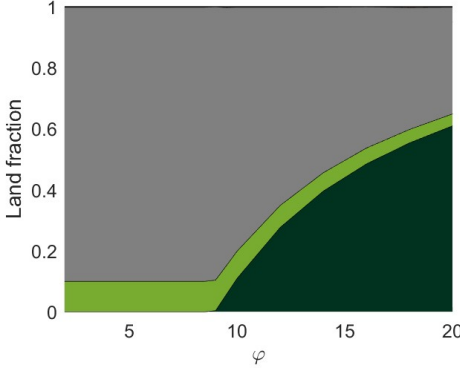


Figure 4: Bifurcation diagram in φ

where the brackets $\langle \cdot \rangle_t$ denote time averages over the time interval $[0, t]$. Thus the stability of GBA trajectories to invasion by forest only depends on time averages of the forest mortality and growth rates along the trajectory.

2.3.2 Estimates of the GBA Steady State

We will now show that using our estimates of the parameter values, the steady state $(\bar{G}, \bar{B}, \bar{A})$ can be easily estimated. Notice that $\mathcal{F}(G)$ becomes asymptotic to $\frac{\gamma q}{\gamma+q}(\frac{1}{G} - \frac{\beta_G}{q})$ as $G \rightarrow 0$ and the coefficient $\frac{\gamma q}{\gamma+q}$ is of order 2. Since $\Phi_G(G)$ is of order 0 or lower for $G \in [0, 1]$ then we can approximate the condition $\Phi_G(G) = \mathcal{F}(G)$ as $0 = \mathcal{F}(G)$ which gives $\bar{G} \approx \frac{q}{\beta_G}$. It follows that to increase the portion of land covered in grass we must either increase q , i.e. increasing the fire quenching rate, or decrease β_G , i.e. decreasing the rate of fire spread through grass, both of which make sense intuitively. By solving System 7 and using $G + B + A = 1$ we can compute an estimate of the GBA steady state as well as the ratio \bar{B}/\bar{A} :

$$(\bar{G}, \bar{B}, \bar{A}) \approx \left(\frac{q}{\beta_G}, \frac{\gamma(1 - \frac{q}{\beta_G})}{q + \gamma}, \frac{q(1 - \frac{q}{\beta_G})}{q + \gamma} \right) \iff \frac{\bar{B}}{\bar{A}} \approx \frac{\gamma}{q}. \quad (10)$$

Based on the estimate, the ratio between the portions of land in burning and ash states is determined by γ , the rate of grass regrowth from ash, and q , the rate of fire quenching in a manner that agrees with intuition.

Then Equation 10 can be used to give Condition 9 purely in terms of the model parameters:

$$\frac{\beta_F \gamma (1 - \frac{q}{\beta_G})}{q + \gamma} + \Phi_F \left(\frac{q}{\beta_G} \right) + \mu > \frac{q \varphi_G}{\beta_G} + \frac{q \varphi_A (1 - \frac{q}{\beta_G})}{q + \gamma}. \quad (11)$$

In particular, if we vary each of the parameters $\beta_F, \gamma, f_0, \mu$, and $\varphi = \varphi_A = \varphi_G$ one at a time and fix all other parameters at the estimates given in Table 3, we can compute the transcritical bifurcation points for each parameter. To simplify the calculations, we will treat Φ_F as a Heaviside step function, that is

$$\Phi_F(x) = f_0 + (f_1 - f_0)H(x - \theta) \quad \text{where} \quad H(x) = \begin{cases} 1 & x \geq 0 \\ 0 & x < 0 \end{cases}$$

which can be viewed as Φ_F in the limit $s_F \rightarrow 0$.

2.4 FGBA Model Steady States

We next solve for the FGBA steady states. We first use $A = 1 - F - G - B$ to eliminate F from Equations 4 to 6 which gives the following system of equations:

$$\dot{F}(t) = (1 - F - B)\varphi F - \beta_F BF - \Phi_F(G)F - \mu F \quad (12)$$

$$\dot{G}(t) = \gamma(1 - F - G - B) + \mu F - \varphi FG - \Phi_G(G)G - \beta_G BG \quad (13)$$

$$\dot{B}(t) = \Phi_G(G)G + \Phi_F(G)F + (\beta_G G + \beta_F F)B - qB. \quad (14)$$

Note that from this point forward we will set $\varphi = \varphi_A = \varphi_G$ to simplify calculations. This is an ecologically reasonable assumption since the rate of forest spread into ash should not differ substantially from the rate of forest spread into grassland. Note that a similar assumption was made [18]. Then after setting $\dot{G} = \dot{B} = \dot{A} = 0$ we can solve for roots $(\bar{F}, \bar{G}, \bar{B}, \bar{A})$. Analogously to the GBA system, we can first check for flow invariance of the tetrahedron $\mathcal{T}_{FGBA} = \{(F, G, B) \mid F \geq 0, G \geq 0, B \geq 0, F + G + B \leq 1\}$ to ensure that any trajectory starting at an ecologically relevant condition remains ecologically relevant at all times.

$$\begin{cases} F = 0 & \Rightarrow \dot{F} = 0 \\ G = 0 & \Rightarrow \dot{G} = \gamma(1 - F - B) + \mu F \geq 0 \\ B = 0 & \Rightarrow \dot{B} = \Phi_G(G)G + \Phi_F(G)F \geq 0 \\ F + G + B = 1 & \Rightarrow \dot{F} + \dot{G} + \dot{B} = -qB \leq 0 \end{cases}$$

With the full system in hand we can now investigate the transcritical bifurcation that occurs at the transition from the GBA steady state to states with non-zero forest. Let $\bar{B}(F)$ be a function that outputs the equilibrium burning proportion(s) B for any given input F . The function $\bar{B}(F)$ can be obtained from Equations 12 to 14 by solving for B in terms of F after setting $\dot{G} = \dot{B} = 0$ and enforcing $F + G + B + A = 1$. In general, $\bar{B}(\cdot)$ is a complicated function that we will analyze in more detail later. The vector field for forest cover can be expressed as

$$\begin{aligned} Q(F) &= (1 - F - \bar{B}(F))F\varphi - \beta_F \bar{B}(F)F - (f_1 + \mu)F \\ &= -\bar{B}(F)F(\varphi + \beta_F) - \varphi F^2 + F(\varphi - \tilde{\mu}) \end{aligned}$$

where we introduce the parameter $\tilde{\mu} := \mu + f_1$ to reduce notational clutter. The normal form for a transcritical bifurcation is $\dot{x} = a_1 x + x^2$. To verify that the generacy conditions for a transcritical bifurcation hold we note first note that $Q(F=0) = 0$ as expected since $F=0$ is an equilibrium. Furthermore,

$$Q'(F=0) = -\bar{B}(0)(\varphi + \beta_F) + \varphi - \tilde{\mu}$$

which indicates the stability of the $F=0$ equilibrium (i.e. the GBA equilibrium). For instance, note that the inequality $Q'(F) < 0$ is exactly the same as Condition 9 after making the simplifications $\varphi = \varphi_G = \varphi_A$ and $\Phi_F(\bar{G}) = f_1$. Lastly, we have

$$Q''(0) = -2\bar{B}'(0)(\varphi + \beta_F) - 2\varphi$$

and it follows that as long as $Q''(0) \neq 0$ a non-degenerate transcritical bifurcation occurs at parameter values where $Q'(F=0)$ i.e. when

$$\bar{B}(0) = \frac{\varphi - \tilde{\mu}}{\varphi + \beta_F} \quad (15)$$

Next, we know that after passing the transcritical bifurcation the system displays two distinct equilibria, one of which is stable while the other is unstable. Since $F = 0$ is always an equilibrium, it remains to be determined whether or not the second equilibrium is ecologically plausible i.e. contained in \mathcal{F}_{FGBA} . To do this we first note that the nonzero forest equilibrium can be calculated from Eqn. (12) by dividing out the factor of F and setting $\dot{F} = 0$. This gives an implicit equation

$$\overline{F}(\overline{B}) = \frac{(\varphi - \tilde{\mu}) - (\varphi + \beta_F)\overline{B}(\overline{F})}{\varphi}.$$

Next we can expand about the equilibria by writing $F = 0 \rightarrow \delta F$ while $\varphi \rightarrow \varphi + \delta\varphi$ or $\beta_F \rightarrow \beta_F + \delta\beta_F$ or $\tilde{\mu} \rightarrow \tilde{\mu} + \delta\tilde{\mu}$. Then, after keeping only first order terms, we find that

$$\left(\frac{\varphi}{\varphi + \beta_F} + \overline{B}'(0) \right) \delta F = \left(\frac{\tilde{\mu} + \beta_F}{(\varphi + \beta_F)^2} \right) \delta\varphi = \left(\frac{\tilde{\mu} - \varphi}{(\varphi + \beta_F)^2} \right) \delta\beta_F = \left(\frac{-1}{(\varphi + \beta_F)^2} \right) \delta\tilde{\mu}.$$

Then the new equilibria emerging at the transcritical point after perturbation of a parameter value is ecologically plausible exactly when $\delta F > 0$. Thus, whether or not the non-zero forest equilibria is ecologically plausible can be determined based on the parameter values $\tilde{\mu}, \beta_F, \varphi$ as well as $\overline{B}'(0)$.

We now examine the function $\overline{B}(F)$ which takes the form

$$\overline{B}(F) = \frac{a_2 F^2 + a_1 F + a_0 \pm \sqrt{b_4 F^4 + b_3 F^3 + b_2 F^2 + b_1 F + b_0}}{c_1 F + c_0}$$

where the coefficients are functions of the parameters $\beta_F, \beta_G, \gamma, q, g_1, g_1, \mu$, and φ . The following coefficients will be particularly useful:

$$\begin{aligned} a_1 &= g_1 \beta_F + \tilde{\mu} \beta_G + \beta_F \gamma - \beta_G \gamma - q \varphi \\ a_0 &= g_1 q - g_1 \gamma - q \gamma + \beta_G \gamma \\ b_1 &= -2g_1^2 \beta_F (q + \gamma) + 2f_1 g_1 \beta_G (q + \gamma) - 4g_1 q \beta_F \gamma + 2f_1 q \beta_G \gamma - 2g_1 \beta_F \beta_G \gamma_2 f_1 \beta_G^2 \gamma - 2g_1 \beta_F \gamma^2 - 2q \\ b_0 &= ((q + \beta_G) \varphi + g_1 (q + \gamma))^2 - 4\beta_G q \varphi^2 \\ c_1 &= -2\beta_F \beta_G \\ c_0 &= 2\beta_G (q + \gamma). \end{aligned}$$

We are interested in the behavior of $\overline{B}(F)$ for $F \approx 0$ to first order in F , so it suffices to Taylor expand the numerator about $F = 0$ to first order in F so that $\overline{B}(F)$ may be sufficiently approximated by a rational function:

$$\overline{B}(F) \approx \frac{a_1^* F + a_0^*}{c_1 F + c_0}$$

where the coefficients a_0^* and a_1^* are computed as

$$(a_0^*, a_1^*) = \left(a_0 \pm \sqrt{b_0}, a_1 \pm \frac{b_1}{2\sqrt{b_0}} \right).$$

A continuity argument with the GBA case will be used to show that we should choose the plus sign. Then we can immediately read that

$$\overline{B}(0) = \frac{a_0^*}{c_0} = \frac{a_0 + \sqrt{b_0}}{c_0} \tag{16}$$

$$\overline{B}'(0) = \frac{c_0 a_1^* - c_1 a_0^*}{c_0^2} = \frac{1}{c_0} \left(a_1 + \frac{b_1}{2\sqrt{b_0}} - c_1 \overline{B}(0) \right). \tag{17}$$

To show that we should choose the plus sign we compute the coefficient a_0^* to zeroth order in g_1 :

$$a_0^* = \gamma(\beta_G - q) \pm \gamma(\beta_G - q) + \mathcal{O}(g_1).$$

so that in the $g_1 \rightarrow 0$ limit

$$\bar{B}(0) \rightarrow \frac{\gamma(\beta_G - q) \pm \gamma(\beta_G - q)}{2\beta_G(q + \gamma)}.$$

We expect in the $g_1 \rightarrow 0$ limit that $\bar{B}(0)$ should match the same result as the $\Phi_G(G) = 0$ approximation we made earlier in the GBA case (see Eqn. (10)) so we must take the plus sign. In general, $\bar{B}(0)$ is a complicated radical expression which is difficult to interpret intuitively in its exact form. However, since the g_1 parameter is small relative to γ, β_G , and q we can approximate $\bar{B}(0)$ as a series in g_1 :

$$\bar{B}(0) = \frac{\gamma(\beta_G - q)}{\beta_G(q + \gamma)} + \frac{qg_1}{\beta_G(\beta_G - q)} + \frac{q(q + \gamma)g_1^2}{(q - \beta_G)^3\gamma} + \mathcal{O}(g_1^3). \quad (18)$$

Then the parameter values along which the transcritical bifurcation occurs can be determined using Eqns. (19) and (18) to various corrections in orders of g_1 :

$$\frac{\varphi - \tilde{\mu}}{\varphi + \beta_F} = \frac{\gamma(\beta_G - q)}{\beta_G(q + \gamma)} + \frac{qg_1}{\beta_G(\beta_G - q)} + \frac{q(q + \gamma)g_1^2}{(q - \beta_G)^3\gamma} + \mathcal{O}(g_1^3) \quad (19)$$

A plot of numerically computed branch points along with the equations above is given in Fig. (5).

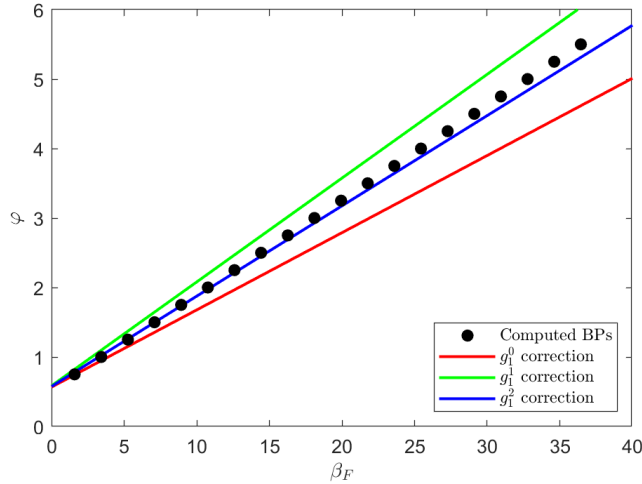


Figure 5: A plot of the computed branch points governing the stable to unstable transition for the GBA steady state alongside the analytically predicted branch points in Eqn. (19). The following toy parameter values were used: $\beta_G = 50$, $\beta_F = 10$, $q = 30$, $\gamma = 10$, $\varphi = 0.1$, $f_0 = g_0 = 0.01$, $f_1 = 0.5$, $g_1 = 1$

Similarly, we can compute $\bar{B}'(0)$ using Eqn. (18). As this expression is quite complicated we only provide here the limit where $f_1 \rightarrow 0, g_1 \rightarrow 0$:

$$\bar{B}'(0) \approx \frac{1}{c_0} \left(a_1 + \frac{b_1}{2\sqrt{b_0}} - c_1 \bar{B}(0) \right).$$

2.4.1 Bifurcation diagrams

As can be seen from the previous section, the analytical analysis of the FGBA system with non-zero forest is rather complicated. As such, a numerical study of the system is useful for a more general understanding of

the system's behavior. Unfortunately, numerical computations with timescale-separated parameter values is extremely slow. Thus, we performed a numerical analysis with somewhat less timescale-separated parameter values: $\beta_G = 50$, $\beta_F = 10$, $q = 30$, $\gamma = 10$, $\varphi = 0.1$, $f_0 = g_0 = 0.01$, $f_1 = 0.5$, $g_1 = 1$.

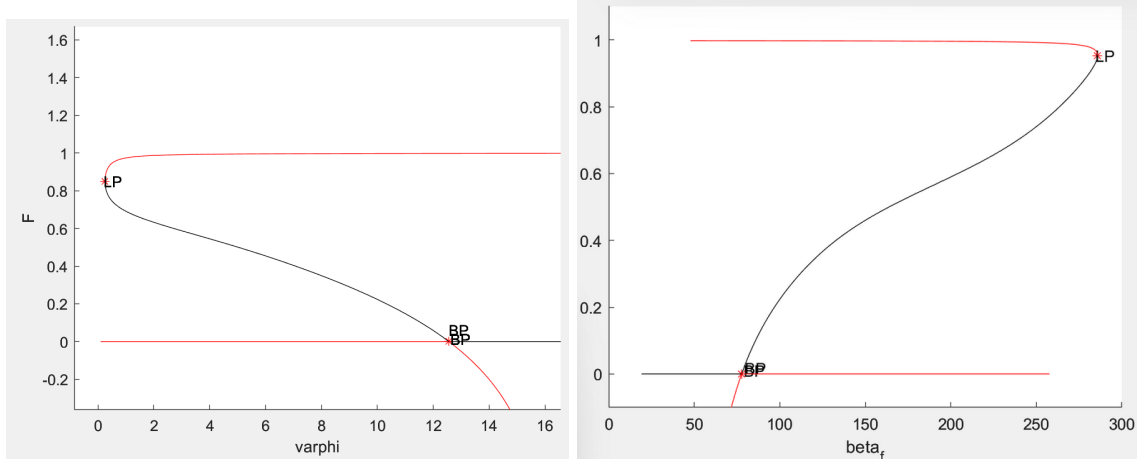


Figure 6: One parameter bifurcation diagrams in φ (left) and β_F (right). Red lines indicate stable equilibria while black lines indicate unstable equilibria.

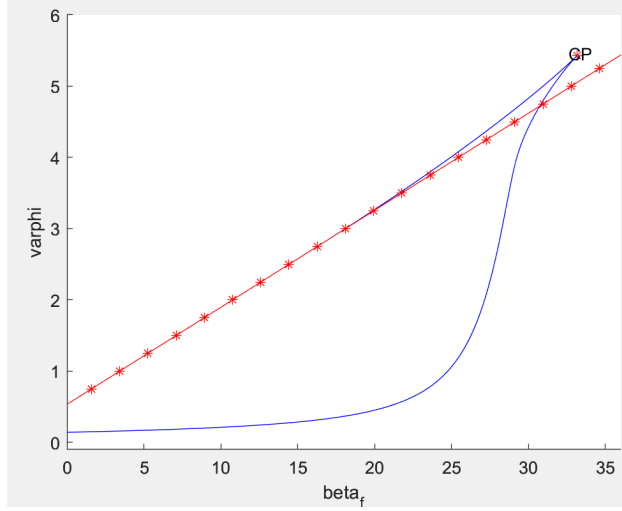


Figure 7: Two-parameter bifurcation diagram for β_F and φ . Limit points are indicated by the blue line. The branch point is indicated by the red line. The branch point line was plotted by interpolating between branch points computed at discrete values of φ and β_F indicated by the red stars.

We note that as expected, the zero forest cover state is stable at low values of φ and high values of β_F . Notably, a stable high forest state is also present in the same parameter ranges as the low forest states. Further, as expected a transcritical bifurcation is present at the critical parameter values of both φ and β_F where the GBA steady state becomes unstable. In the two-parameter bifurcation diagram (Fig. (7)), the region outlined in blue indicates the parameter regimes in which we can expect bistability in forest cover.

3 Simulations of the fully spatial FGBA model

3.1 Algorithms

All code used in this project can be accessed at https://github.com/patterd2/vegetation_fire_models. The spatial FGBA model was simulated in MATLAB using the Gillespie algorithm [21] which provides an exact solution or alternately using Tau leaping [22] to increase simulation speed at the expense of exact accuracy.

3.2 Simulation testing

Before proceeding with analysis of the model we perform some sanity tests on the model to ensure that the code is bug-free and is behaving as predicted. We test each transition rate separately by introducing some artificial simulation situations whose behavior is readily predictable and comparing the simulation results with predictions.

3.2.1 Testing non-spatial transitions

The simplest transitions to test are the spontaneous, non-spatial transitions governed by the parameters q ($B \rightarrow A$), γ ($A \rightarrow G$) and μ ($F \rightarrow G$) corresponding to fire quenching, grass regrowth, and tree mortality, respectively. All testing was performed with $L = 100$ and $N = 500$.

To test the fire quench rate we began the simulation with all states in the burning state and removed grass regrowth by setting $\gamma = 0$. The times at which each burning state transitioned into the ash state were recorded at various values of q . The quench times are expected to follow a Poisson distribution with rate q , giving an expected quench time of $\frac{1}{q}$ with variance $\frac{1}{q}$.

Similarly, to check the grass regrowth rate from ash we began with all sites in the ash state. We set $g_0 = g_1 = 0$ to remove spontaneous grass fires. The times at which each ash site transitioned into a grass state was recorded for various values of γ . As expected, the regrowth times followed a Poisson distribution with rate γ and expected regrowth time $\frac{1}{\gamma}$ with variance $\frac{1}{\gamma}$.

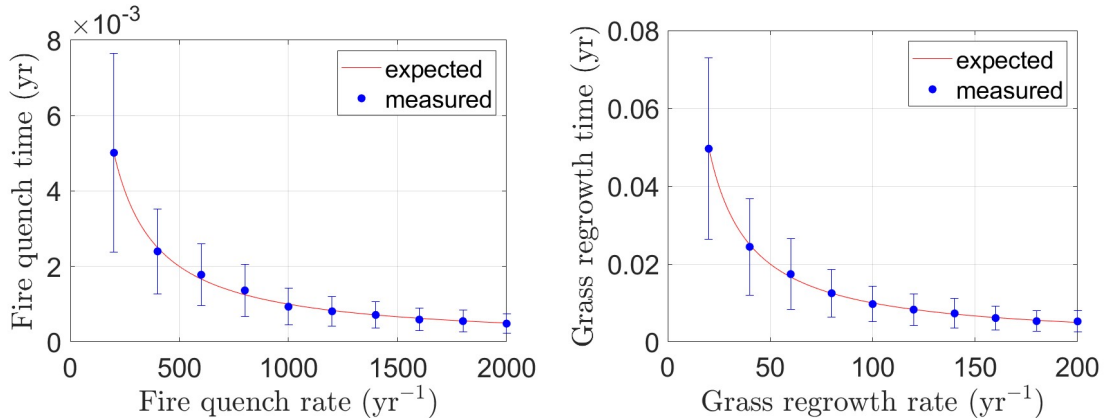


Figure 8: Testing the fire quench transition (left) and the grass regrowth transition (right)

Lastly, to check forest mortality transitions we began the simulation with all sites in the forest state

and removed forest spread by setting $\varphi_G = \varphi_A = 0$. Grass and forest fires were also eliminated by setting $g_0 = g_1 = f_0 = f_1 = 0$. The times at which each forest site transitioned into a grass state was recorded at various values of μ . The tree lifetimes are expected to follow a Poisson distribution with rate μ giving an expected lifetime of $\frac{1}{\mu}$ with variance $\frac{1}{\mu}$.

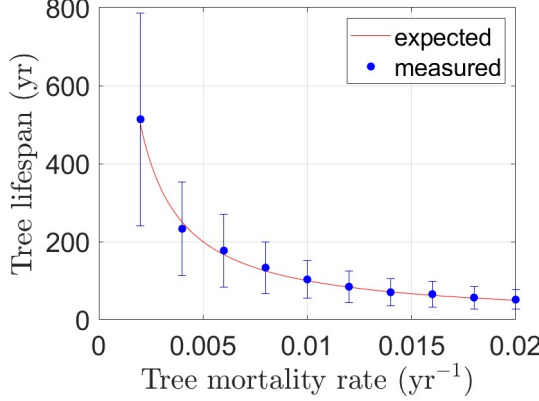


Figure 9: Tree mortality testing

3.2.2 Testing spatial transitions

We next tested the four directly spatial transitions in the FGBA model: the spread of forest through grass and through ash and the spread of fire through grass and through forest.

Fire spread through grass was tested introducing the initial condition where a single randomly chosen vegetation site in the domain would be in a grass state while the remaining sites are all randomly assigned to be either burning or ash states according to some fixed probability p_{ash} of the state being ash. Further, $g_0 = g_1 = \gamma = q = 0$ was set to remove spontaneous grass ignitions and grass regrowth and prevent fire quenching. The burn rate at the grass site is then expected to be approximately $\beta_G p_{\text{ash}}$. The time at which the grass site transitioned to a burning state was then measured at various values of β_G and p_{ash} . The average of five trials for each pair of values $(\beta_G, p_{\text{ash}})$ is plotted in Fig. (10).

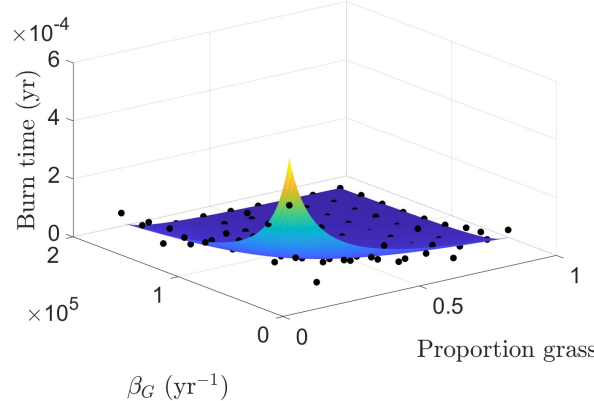


Figure 10: Testing of the spatial transition of grass sites to burning sites

Fire spread through forest was tested in an analogous situation where instead of a single grass site, a single forest site was used and $f_0 = f_1 = \mu = 0$ was set to eliminate all possible transitions except the forest to burning transition. The burn rate at the forest site is then expected to be approximately $\beta_F p_{\text{ash}}$. The time at which the grass site transitioned to a burning state was then measured at various values of β_F and p_{ash} . The average of five trials for each pair of values $(\beta_F, p_{\text{ash}})$ is plotted in Fig. (10).

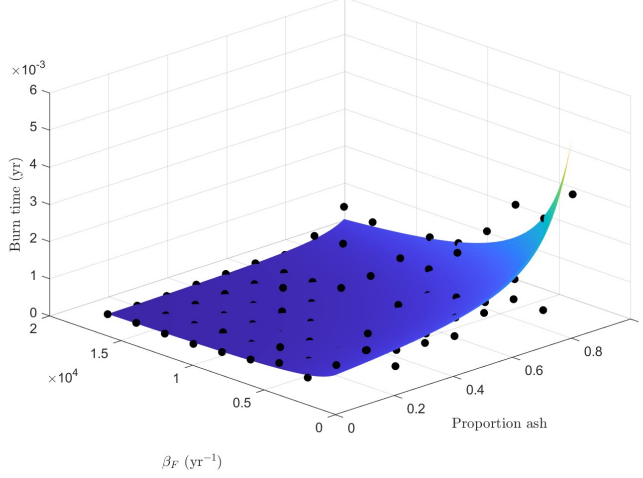


Figure 11: Testing of the spatial transition of forest sites to burning sites

Next, the spread of forest through grass was tested by randomly choosing a single vegetation site to be grass while the remaining sites are randomly chosen to be in the forest state with probability p_{forest} and are otherwise in the ash state. To prevent all other possible transitions besides the grass to forest transition we set $g_0 = g_1 = f_0 = f_1 = q = \gamma = \mu = \varphi_A = 0$. Then the rate at which the grass site should transition to forest is approximately $\varphi_G p_{\text{forest}}$. The time at which the grass site transitioned to a forest state was then measured at various values of φ_G and p_{forest} . The average of five trials for each pair of values $(\varphi_G, p_{\text{forest}})$ is plotted in Fig. (12).

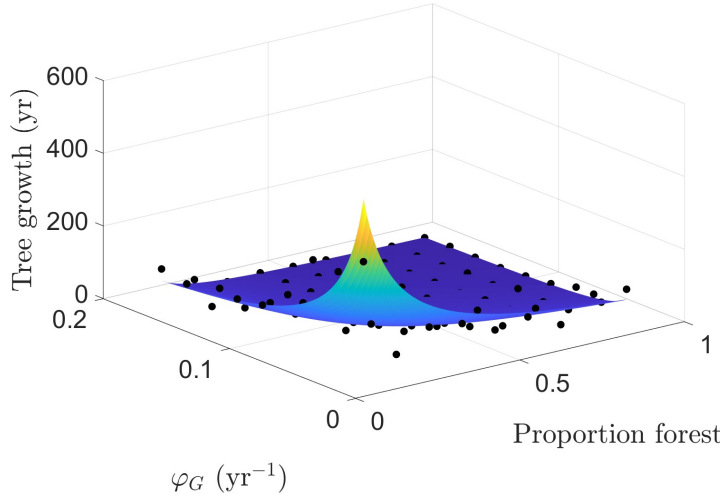


Figure 12: Testing of the spatial transition of grass sites to forest sites

Lastly, the spread of forest through ash was tested by randomly choosing a single vegetation site to be ash while the remaining sites are randomly chosen to be in the forest state with probability p_{forest} and are otherwise in the grass state. To prevent all other possible transitions besides the ash to forest transition we set $g_0 = g_1 = f_0 = f_1 = q = \gamma = \mu = \varphi_G = 0$. Then the rate at which the ash site should transition to forest is approximately $\varphi_A p_{\text{forest}}$. The time at which the grass site transitioned to a forest state was then measured at various values of φ_A and p_{forest} . The average of five trials for each pair of values $(\varphi_A, p_{\text{forest}})$ is plotted in Fig. (13).

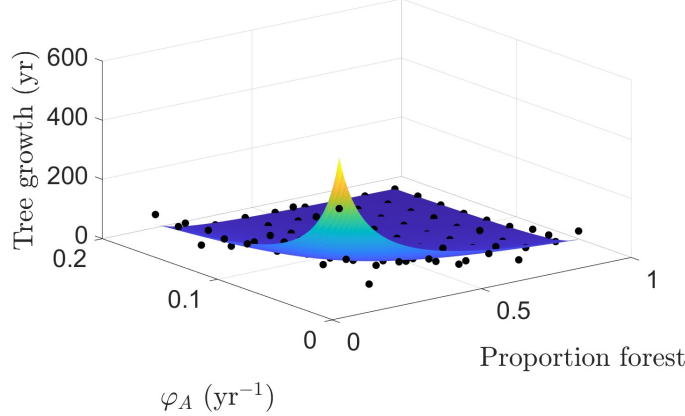


Figure 13: Testing of the spatial transition of ash sites to forest sites

This concludes the testing of the spontaneous and spatial transitions in the FGBA spatial model. In the next section we begin running simulations with time-separated and ecologically-reasonable parameter values in relevant initial conditions.

3.3 Grassland without forest

All simulations in this section and the next section were run with $L = 1$ and $N = 1000$ unless otherwise noted. The use of timescale-separated parameter values enables the FGBA simulation to exhibit a variety of different behaviors that can only be properly observed at vastly differing timescales. For example, the cover proportions of the various states at a fire scale vs a grass time scale is shown in Fig. (14). A montage of the fire depicted on the fire-timescale in Fig. (14) is also shown in Fig. (15).

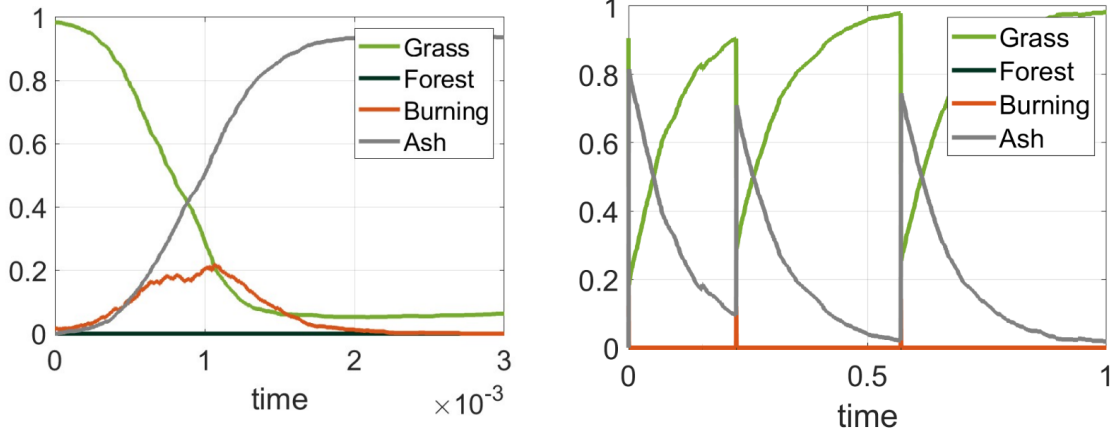


Figure 14: Fire dynamics in grassland at a fire timescale (left) and at a grass timescale (right)

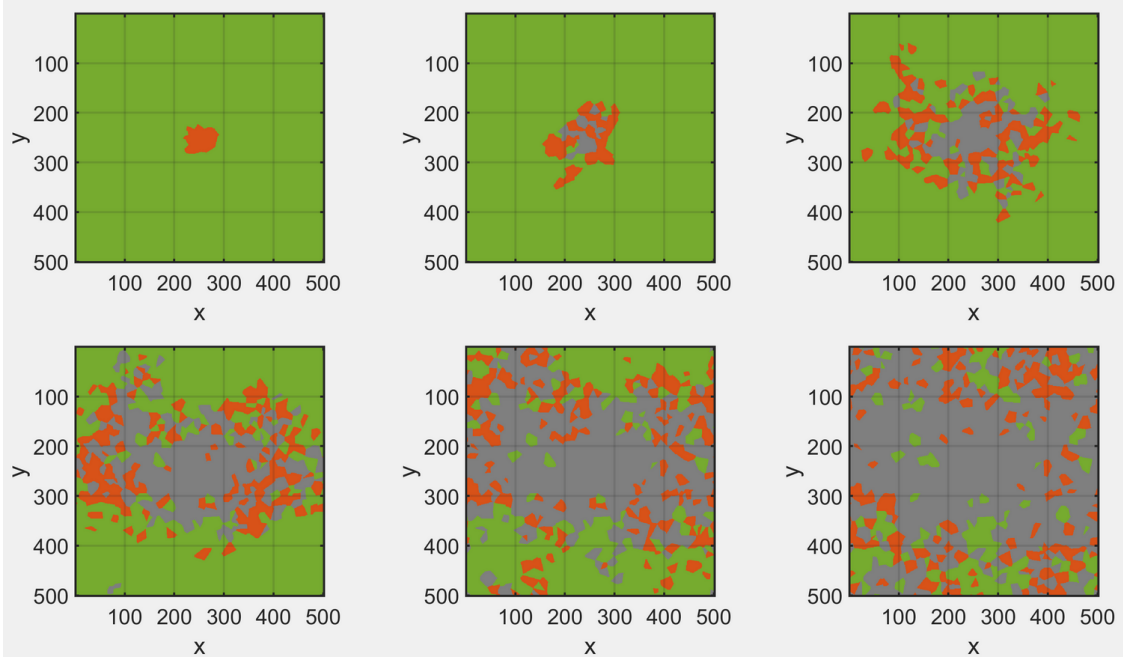


Figure 15: Montage of fire ignition and spreading in grassland on a fire timescale

On the fire timescale, the spatial structure of a fire front spreading through space and leaving behind a region of ash is readily apparent. On the grass timescale, the fire dynamics are obscured but the regrowth of grass following fire spreading events is easily observed. In comparison to the fire spreading, grass regrowth occurs relatively homogeneously spatially as shown in Fig. (16).

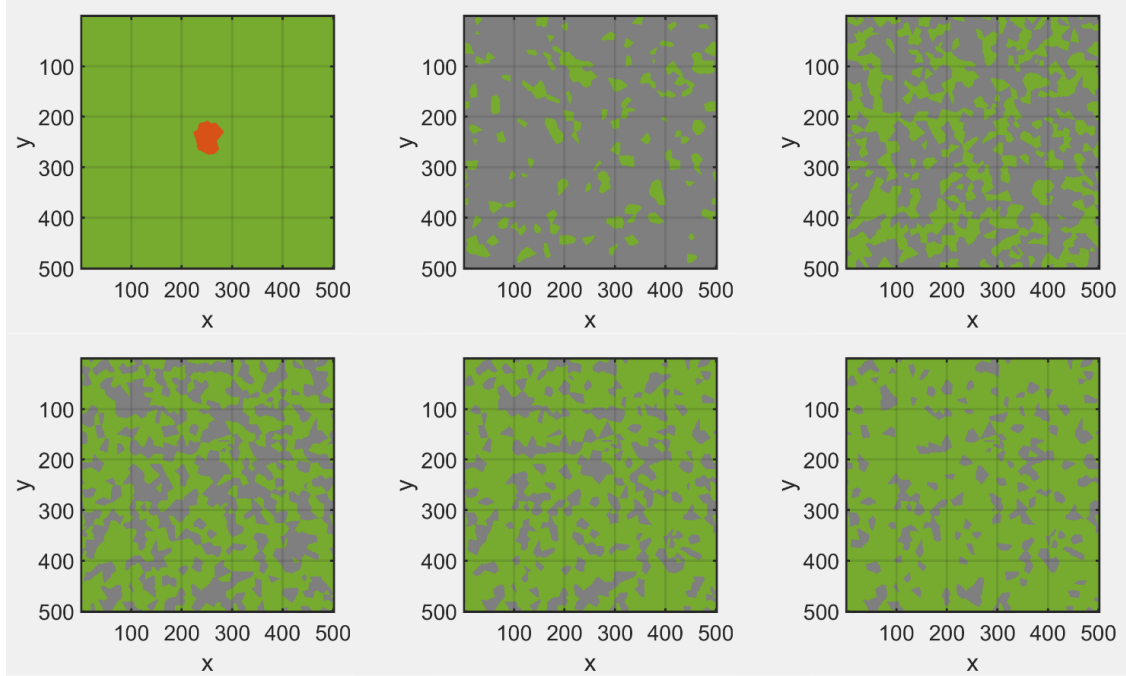


Figure 16: Montage of grass regrowth following a fire ignition event in grassland on a grass timescale

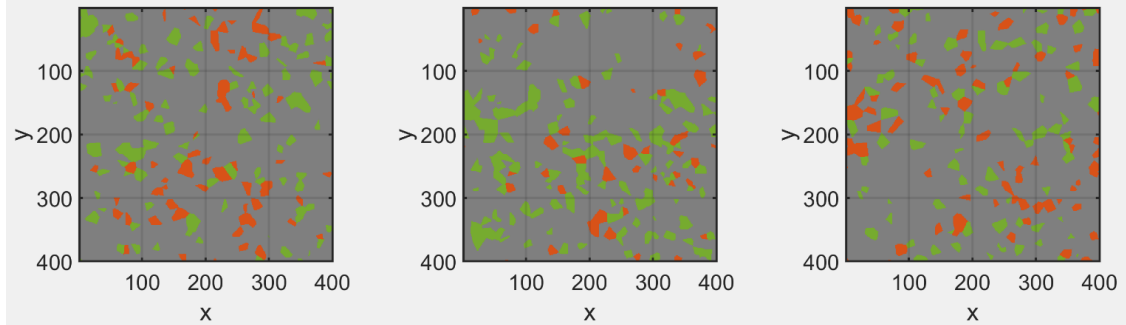


Figure 17: Montage of the system in the mean-field steady state.

Lastly, we note that on the grass timescale, there are several ignition events that occur well-separated in time. This suggests that the spatial model can be viewed as possessing a largely-grass steady state which is distinct from the mean-field steady state which consists of mostly ash. Nonetheless, the spatial model can also demonstrate the mean-field grass steady state under certain conditions. For example, the spatial model can reach the mean-field GBA steady state when q is sufficiently large and when N (equivalently, when σ_{\square} are sufficiently small), γ , and/or β_G is sufficiently small as can be seen in Figs. (18) through (21). In addition, we note that increasing the spontaneous ignition rate of grass results in an increase in frequency of the big fire events as shown in Fig. (22).

As discussed earlier, the mean-field GBA steady state mostly of ash states and is not ecologically realistic. However, the proportions observed in the simulations generally agree with our predictions from the mean-field analysis. Thus, in general, we will use sufficiently large values of q and sufficiently small values of σ_{\square} , γ , and β_G while keeping $N = 1000$ fixed to ensure that the system does not reach the mean-field steady state and maintains spatial structure. A montage of the system in the mean-field steady state is given in Fig. (17).

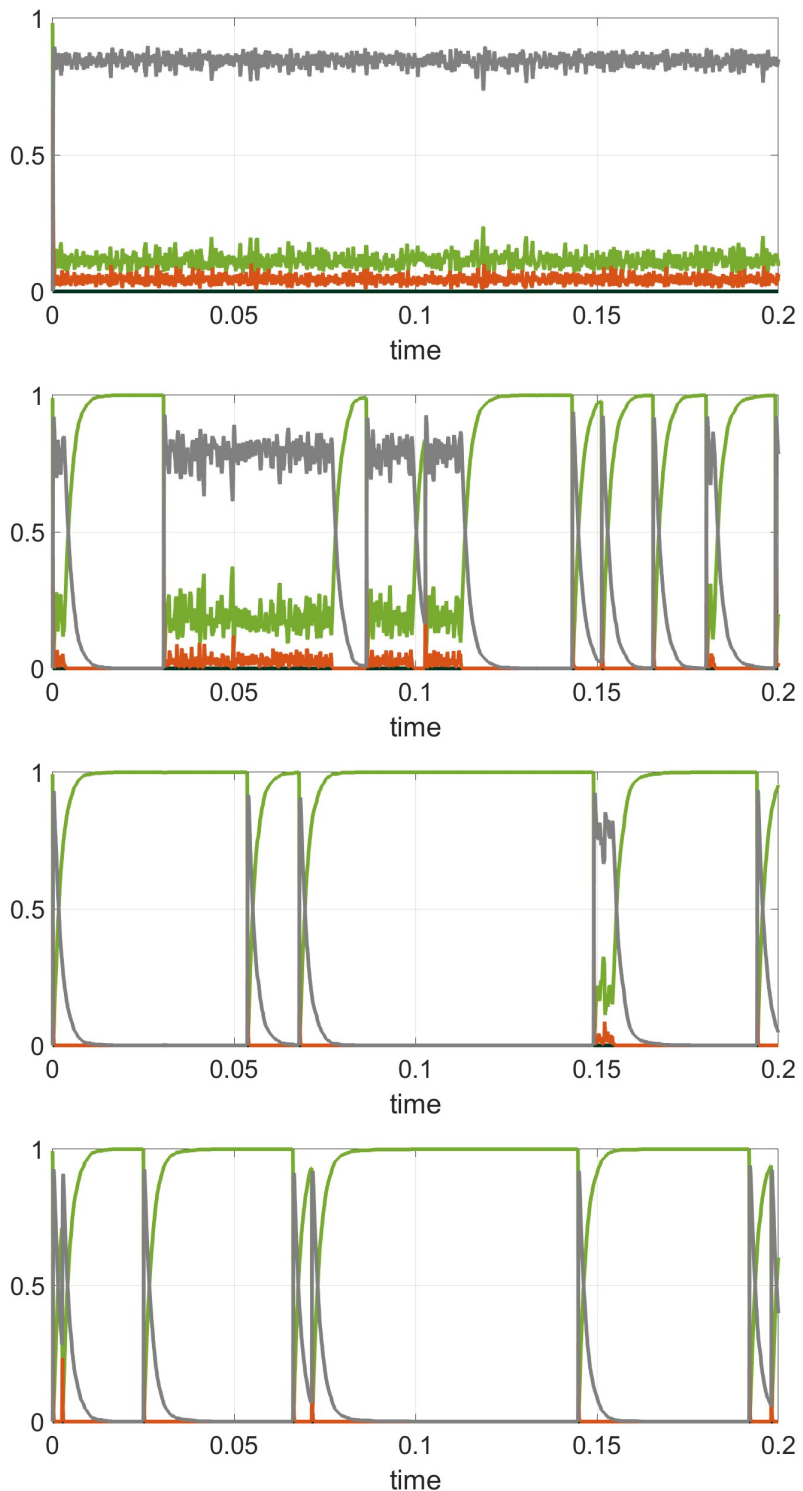


Figure 18: From top to bottom: behavior of grassland for $q = 1.0 \cdot 10^5, 1.6 \cdot 10^5, 1.8 \cdot 10^5$, and $2.0 \cdot 10^5$ while all other parameter values are fixed

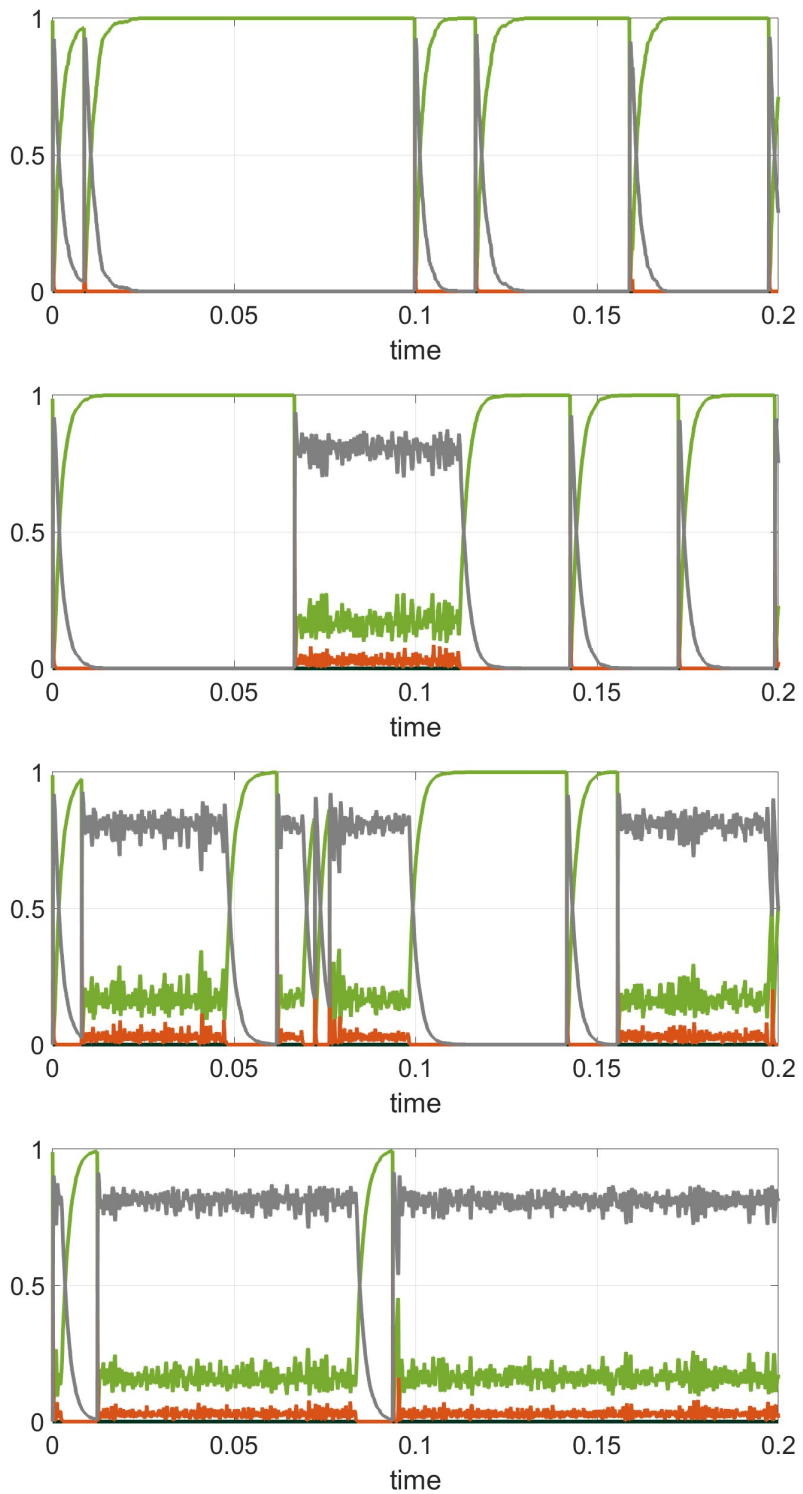


Figure 19: From top to bottom: behavior of grassland for $N = 0.4 \cdot 10^3, 1.1 \cdot 10^3, 1.3 \cdot 10^3$, and $1.8 \cdot 10^3$ while all other parameter values are fixed. The system demonstrates an increased tendency to reach the mean-field steady state at large values of N .

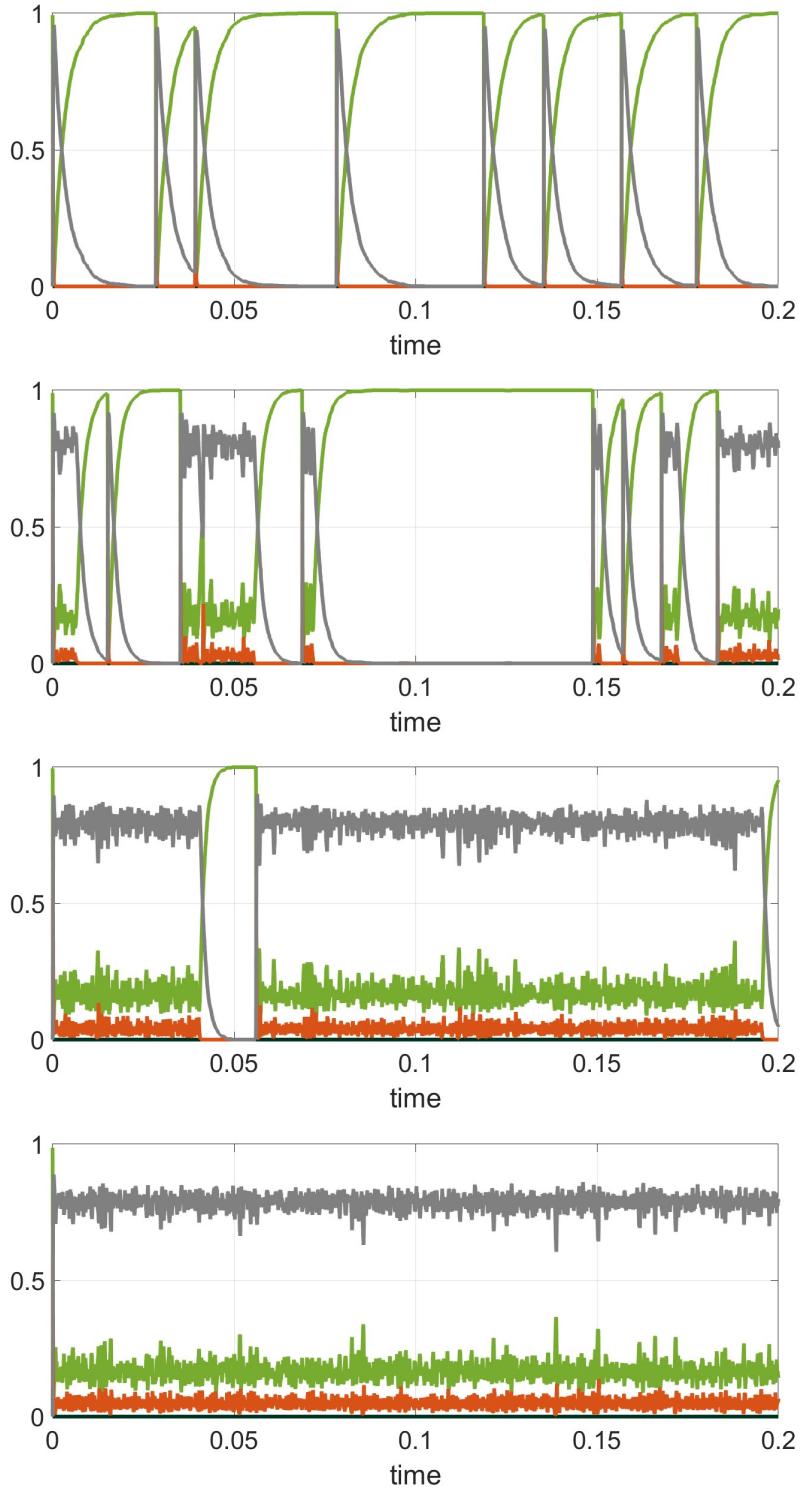


Figure 20: From top to bottom: behavior of grassland for $\gamma = 3.0 \cdot 10^2, 5.0 \cdot 10^2, 7.0 \cdot 10^2$, and $9.0 \cdot 10^2$ while all other parameter values are fixed. The system demonstrates a tendency to reach the mean-field steady state at large values of γ .

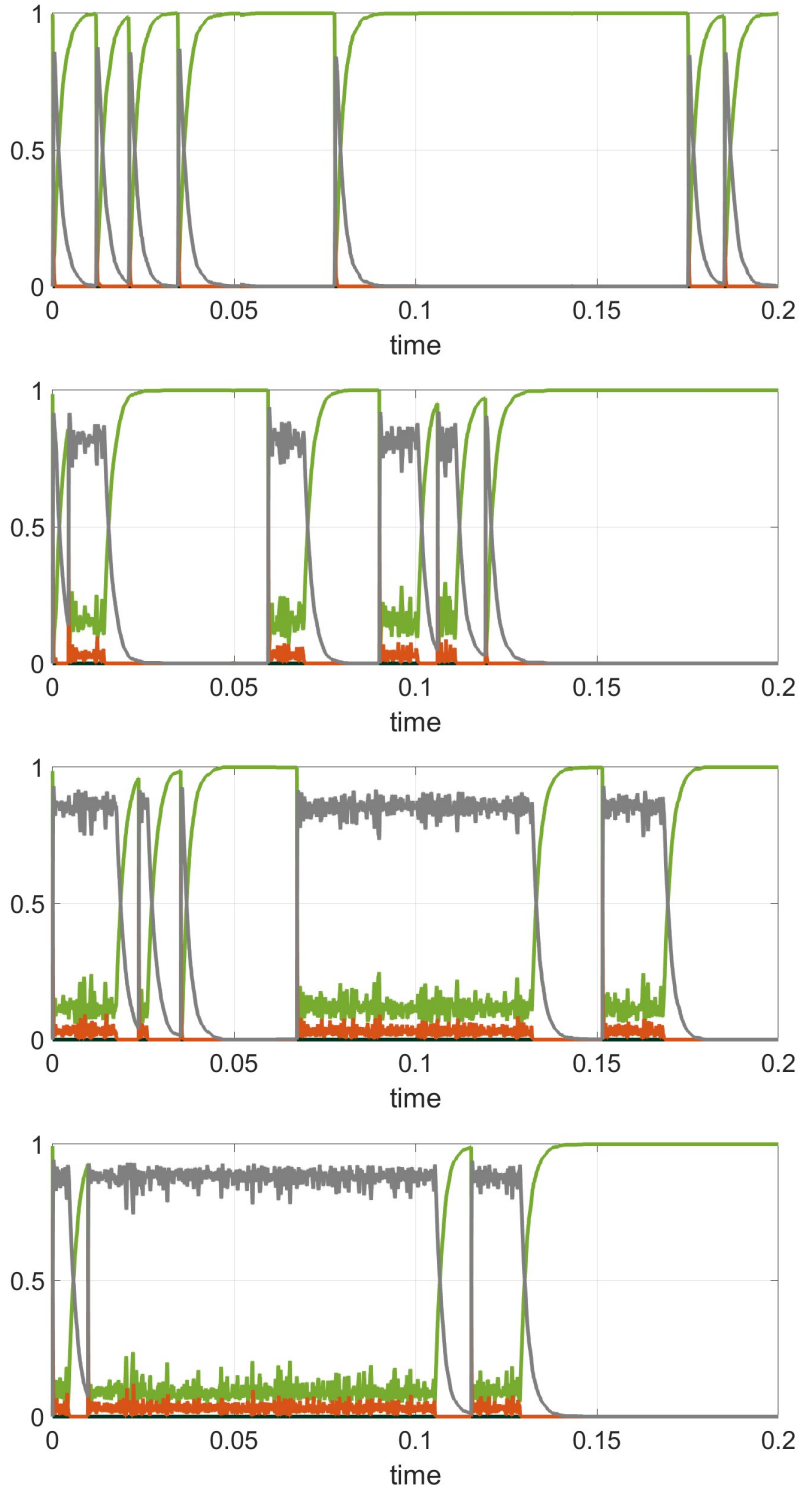


Figure 21: From top to bottom: behavior of grassland for $\beta_G = 0.5 \cdot 10^5, 1.1 \cdot 10^5, 1.5 \cdot 10^5$, and $2.0 \cdot 10^5$ while all other parameter values are fixed. The system demonstrates a tendency to reach the mean-field steady state at large values of β_G .

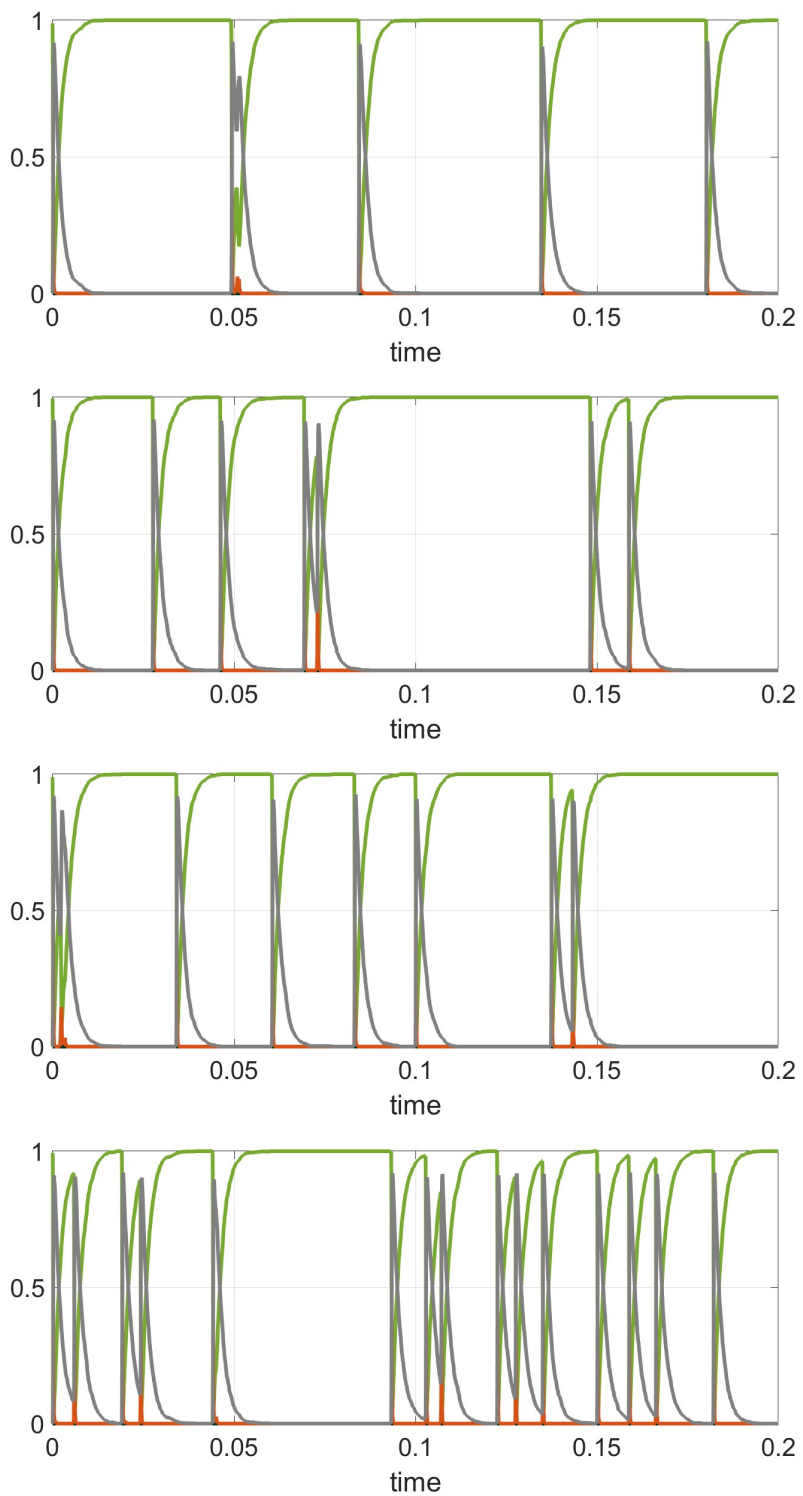


Figure 22: From top to bottom: behavior of grassland for $g_1 = 2.0 \cdot 10^{-2}, 4.0 \cdot 10^{-2}, 7.0 \cdot 10^{-2}$, and $9.0 \cdot 10^{-2}$ while all other parameter values are fixed. The system demonstrates an increased frequency of big fire events as g_1 is increased.

3.4 Grassland with Forest

When studying grassland containing forest we find additional new behavior at the forest timescale. In general, ignition events in grass cause large fires which propagate to an extent determined by the surrounding distribution of forest and destroy trees near the perimeter of the forest regions. During time periods between fire events, the trees steadily regrow.

In general there are two distinct outcomes over longer periods of time. The forest either grows faster than that the transitions that destroy it and eventually becomes so dense that fires can no longer propagate and the high forest state is stably maintained. Alternatively, the grass fires are sufficiently destructive to reduce the forest proportion to a vanishing or near-vanishing proportion at which forest can no longer spread noticeably. These two cases are illustrated in Fig. (23). The final outcome has a stochastic element in the sense that it cannot be determined from the initial conditions of the system alone.

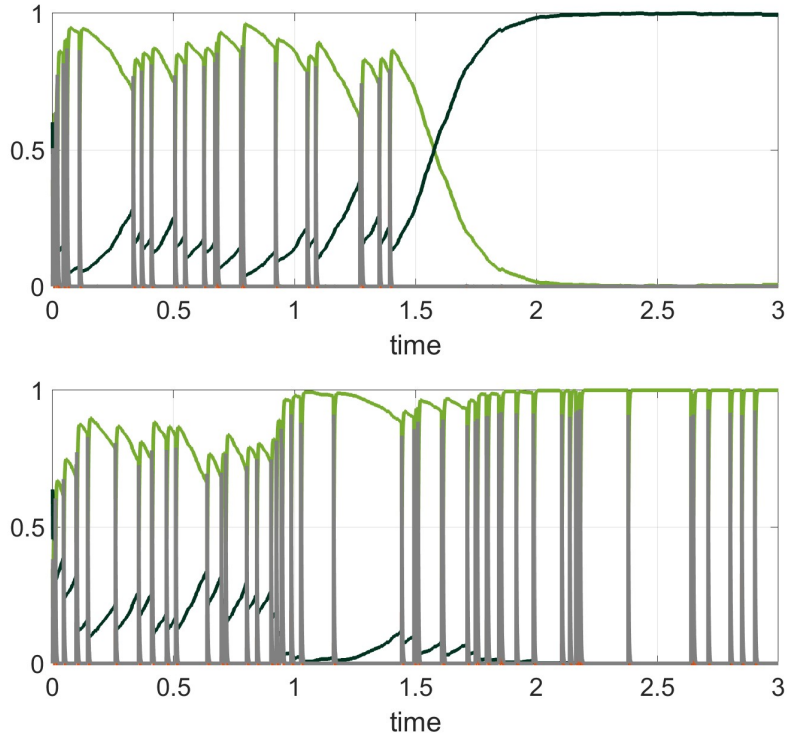


Figure 23: Two different possible outcomes for forest (dark green line). Both systems were run with the same parameter values and initial condition. Forest was randomly distributed and occupied 0.6 of sites. The remaining sites were all grass apart from a small fire patch at $[0.45, 0.55] \times [0.45, 0.55]$.

In simulations starting at an initial condition of high forest cover, there is also a noticeable increase in fire size as the forest cover decreases. An example is shown in Fig. (24). A montage demonstrating the ability of forest cover to limit the extent of fire spreading is given in Fig. (25), corresponding to the fire occurring at the start of the simulation. Relatedly, a montage of increased fire spreading for the fire starting at time $t = 0.53$ at low forest cover is given in Fig. (26).

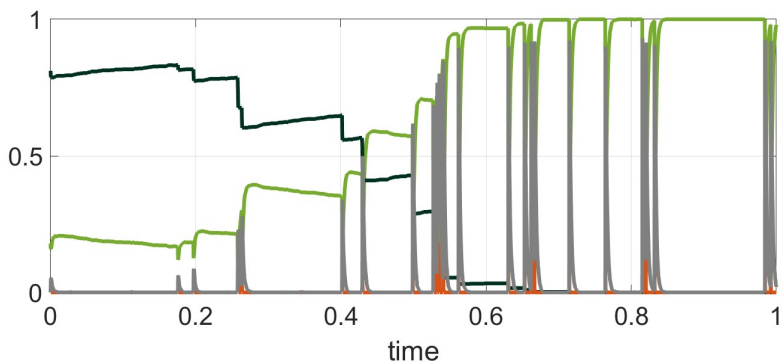


Figure 24: A simulation demonstrating the ability of high forest cover to limit the extent of fire spreading

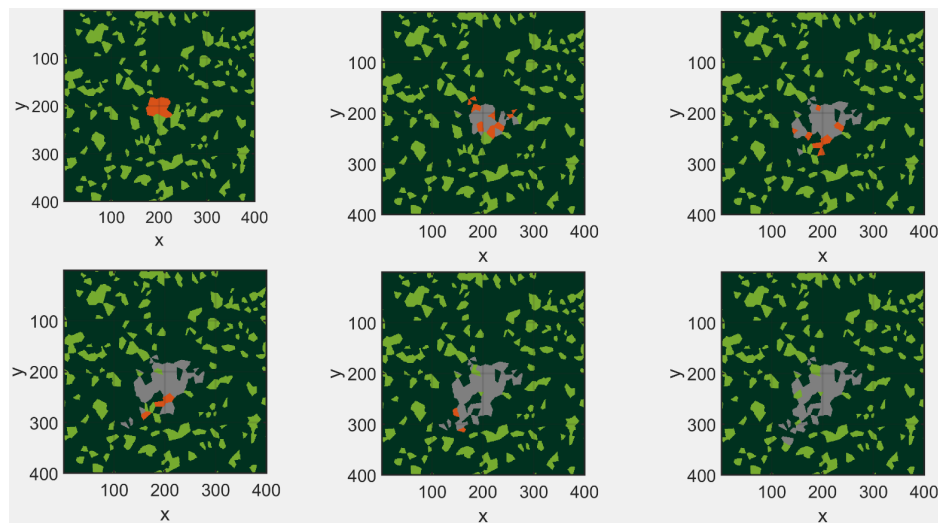


Figure 25: Montage of limited forest fire spread as a result of extensive forest cover at $t = 0$ in Fig. (24)

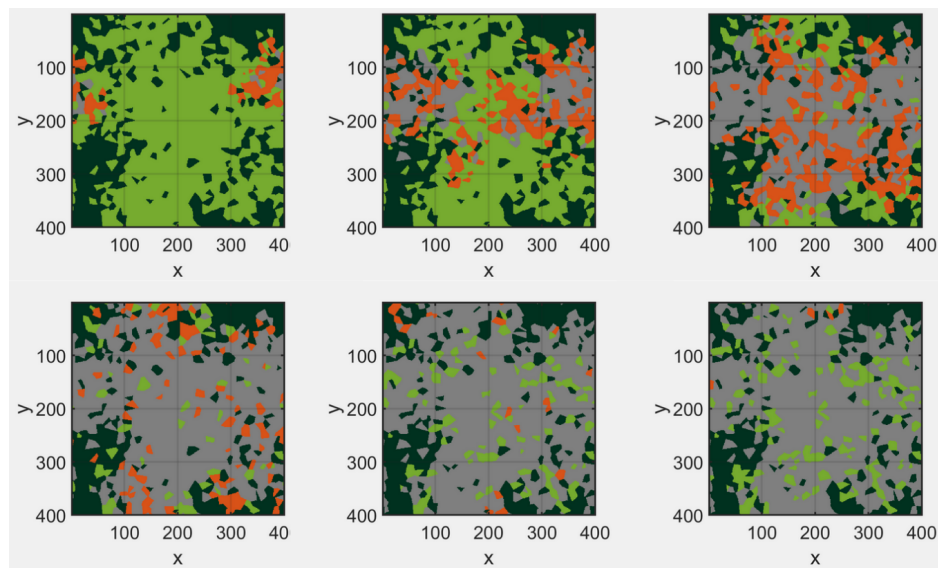


Figure 26: Montage of extensive forest fire spread as a result of low forest cover at $t = 0.53$ in Fig. (24)

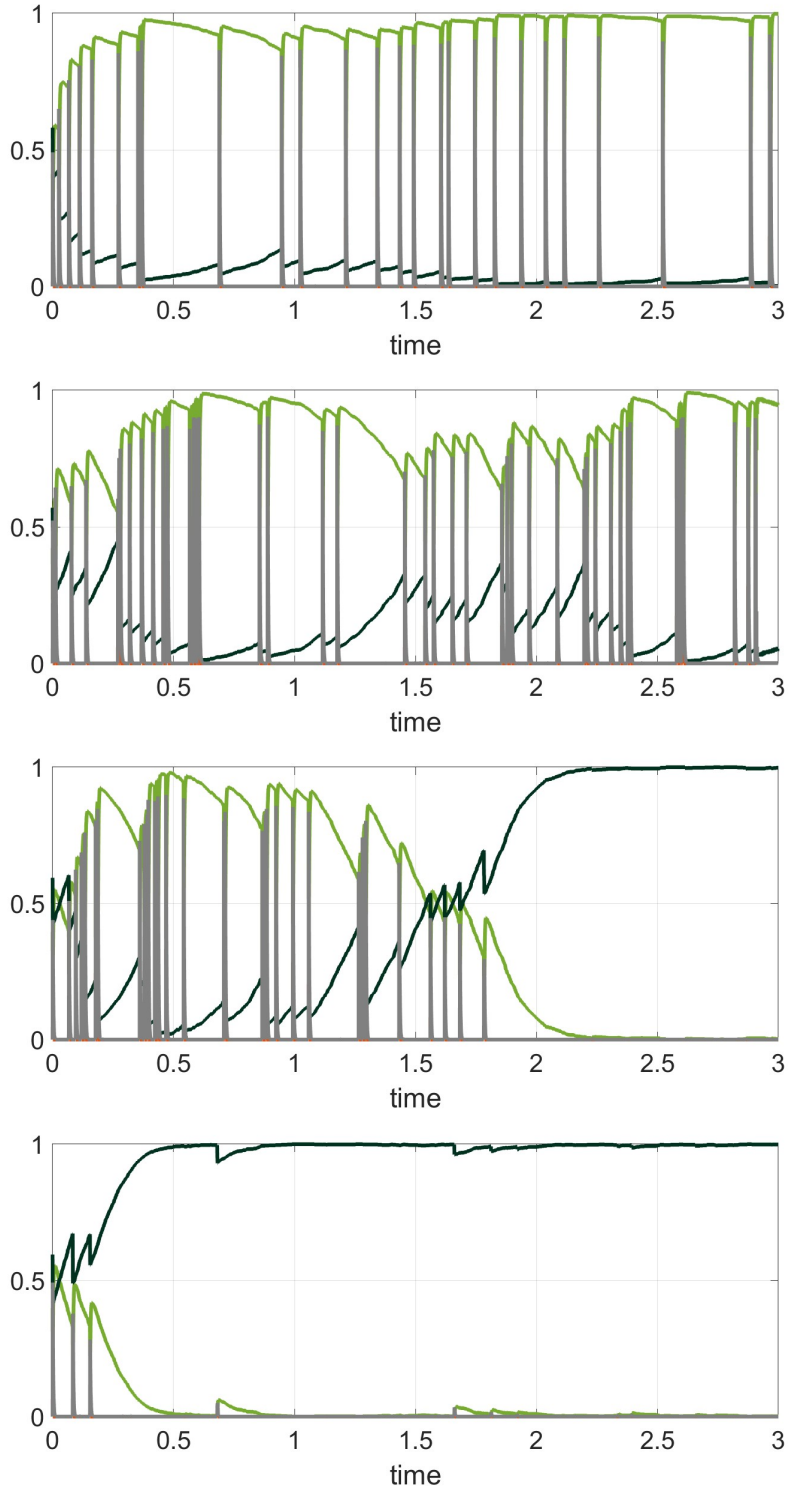


Figure 27: From top to bottom: behavior of forest in grassland for $\varphi = 5, 11, 13, 14$ while all other parameter values are fixed. The initial condition was set with forest randomly occupying 0.6 of the sites. The remaining sites all grass apart from a small fire patch at $[0.45, 0.55] \times [0.45, 0.55]$.

3.5 Conclusions

Overall, we note that the mean-field model provides a reasonably simple method to study the qualitative behavior of the FGBA model but does not necessarily provide numerically accurate results. For instance the stability of the grassland fixed point under parameter regimes with sufficiently high forest mortality is observed in both the mean-field and spatial models. However, the mean-field model predicts only a single grassland fixed point at unrealistically high ash coverage. In contrast, the spatial model demonstrates both a spatially-homogeneous grassland fixed point with high ash coverage as well as additional fixed point characterized by high grass coverage and occasional fire spreading events well-separated in time. In a related example, the stability of forest as a function of the parameter values showed qualitative agreement in both the mean-field and spatial models with increases in parameters such as φ allowing the system to have a finite probability of reaching a high forest state.

In addition, the simulations of the spatial model explicitly demonstrate the hypothesized mechanisms underpinning bistability in forest tree cover. In particular, occasional ignitions followed by rapid fire spreading can maintain low forest cover even at high forest spreading rates. Meanwhile the inability of fire to spread in regions of dense tree cover maintains high forest cover even at high fire ignition and spread rates.

Lastly, we note that our proposed FGBA model is highly versatile and can be used study a wide range of possible forest and grassland setups. For example, differences in soil quality could be modeled by choosing vegetation sites within Ω according to a non-uniform probability distribution. One could also model forest spread via heavy-tailed, non-Gaussian spreading kernels which may be a more accurate model of forest spread than our current assumption that forest trees only spread locally. Lastly, one could also investigate the impact of non-spatially uniform forest distributions, for example if forest was distributed into distinct regions of high tree density separated by regions of low tree density or into shapes with varying perimeter-area ratios. We leave these investigations for future work.

References

- [1] A. C. Staver, S. Archibald, and S. Levin, *Tree cover in sub-Saharan Africa: rainfall and fire constrain forest and savanna as alternative stable states*, Ecology **92**, 1063 (2011).
- [2] A. C. Staver, S. Archibald, and S. A. Levin, *The global extent and determinants of savanna and forest as alternative biome states*, science **334**, 230 (2011).
- [3] A. C. Staver and S. A. Levin, *Integrating theoretical climate and fire effects on savanna and forest systems*, The American Naturalist **180**, 211 (2012).
- [4] E. Schertzer, A. Staver, and S. A. Levin, *Implications of the spatial dynamics of fire spread for the bistability of savanna and forest*, Journal of mathematical biology **70**, 329 (2015).
- [5] D. D. Patterson, S. A. Levin, C. Staver, and J. D. Touboul, *Probabilistic foundations of spatial mean-field models in ecology and applications*, SIAM journal on applied dynamical systems **19**, 2682 (2020).
- [6] W. A. Hoffmann, B. Orthen, and P. K. V. Do Nascimento, *Comparative fire ecology of tropical savanna and forest trees*, Functional Ecology , 720 (2003).
- [7] W. A. Hoffmann *et al.*, *Tree topkill, not mortality, governs the dynamics of savanna–forest boundaries under frequent fire in central Brazil*, Ecology **90**, 1326 (2009).
- [8] J. K. Balch *et al.*, *Size, species, and fire behavior predict tree and liana mortality from experimental burns in the Brazilian Amazon*, Forest Ecology and Management **261**, 68 (2011).
- [9] W. A. Hoffmann *et al.*, *Ecological thresholds at the savanna-forest boundary: how plant traits, resources and fire govern the distribution of tropical biomes*, Ecology letters **15**, 759 (2012).
- [10] K. J. Hennenberg *et al.*, *Phytomass and fire occurrence along forest–savanna transects in the Comoé National Park, Ivory Coast*, Journal of tropical ecology **22**, 303 (2006).
- [11] S. Archibald, D. P. Roy, B. W. van Wilgen, and R. J. Scholes, *What limits fire? An examination of drivers of burnt area in Southern Africa*, Global Change Biology **15**, 613 (2009).
- [12] S. Pueyo *et al.*, *Testing for criticality in ecosystem dynamics: the case of Amazonian rainforest and savanna fire*, Ecology letters **13**, 793 (2010).
- [13] W. A. Hoffmann *et al.*, *Fuels or microclimate? Understanding the drivers of fire feedbacks at savanna–forest boundaries*, Austral Ecology **37**, 634 (2012).
- [14] K. J. Hennenberg *et al.*, *Detection of seasonal variability in microclimatic borders and ecotones between forest and savanna*, Basic and Applied Ecology **9**, 275 (2008).
- [15] S. Archibald, A. C. Staver, and S. A. Levin, *Evolution of human-driven fire regimes in Africa*, Proceedings of the National Academy of Sciences **109**, 847 (2012).
- [16] T. Gebele, *Site percolation threshold for square lattice*, Journal of Physics A: Mathematical and General **17**, L51 (1984).
- [17] L. Hébert-Dufresne *et al.*, *Edge fires drive the shape and stability of tropical forests*, Ecology letters **21**, 794 (2018).

- [18] B. Wuyts and J. Sieber, *Emergent structure, dynamics and abrupt transitions in a cellular automaton of tropical forest and fire*, (2023).
- [19] J. D. Touboul, A. C. Staver, and S. A. Levin, *On the complex dynamics of savanna landscapes*, Proceedings of the National Academy of Sciences **115**, E1336 (2018).
- [20] L. Edelstein-Keshet, *Mathematical models in biology* (SIAM, 2005).
- [21] D. T. Gillespie, *Exact stochastic simulation of coupled chemical reactions*, The journal of physical chemistry **81**, 2340 (1977).
- [22] D. T. Gillespie, *Approximate accelerated stochastic simulation of chemically reacting systems*, The Journal of chemical physics **115**, 1716 (2001).